nature human behaviour

Article

https://doi.org/10.1038/s41562-024-01838-3

The direction of theta and alpha travelling waves modulates human memory processing

Received: 14 July 2023

Accepted: 24 January 2024

Published online: 8 March 2024

Check for updates

Uma R. Mohan [1], Honghui Zhang [2], Bard Ermentrout [3] & Joshua Jacobs [4,5]

To support a range of behaviours, the brain must flexibly coordinate neural activity across widespread brain regions. One potential mechanism for this coordination is a travelling wave, in which a neural oscillation propagates across the brain while organizing the order and timing of activity across regions. Although travelling waves are present across the brain in various species, their potential functional relevance has remained unknown. Here, using rare direct human brain recordings, we demonstrate a distinct functional role for travelling waves of theta- and alpha-band (2–13 Hz) oscillations in the cortex. Travelling waves propagate in different directions during separate cognitive processes. In episodic memory, travelling waves tended to propagate in a posterior-to-anterior direction during successful memory encoding and in an anterior-to-posterior direction during recall. Because travelling waves of oscillations correspond to local neuronal spiking, these patterns indicate that rhythmic pulses of activity move across the brain in different directions for separate behaviours. More broadly, our results suggest a fundamental role for travelling waves and oscillations in dynamically coordinating neural connectivity, by flexibly organizing the timing and directionality of network interactions across the cortex to support cognition and behaviour.

The brain supports a diverse range of behaviours, which requires the coordination of neural activity between different sets of regions. How does the brain support this flexibility? One potential mechanism for flexibly organizing large-scale neuronal activity is a travelling wave (TW), which is a neural oscillation that propagates across the cortex[1,2]. TWs are widespread in the brain, appearing across multiple regions in animals[3–7] and humans[8–10], at both small[11–14] and large[10,15–18] scales. Because TWs correlate with local neuronal activity, their spatiotemporal organization indicates which cortical regions are active and in which direction activity is propagating at each moment[4,15]. Furthermore, due to TWs' ability to rapidly reorganize[19], they may support the brain's ability to dynamically adapt its processes to meet changing cognitive demands[20,21]. However, despite these theoretical features and TWs' widespread prevalence[2,15], their behavioural importance is unknown. Our goal here was thus to identify potential functional roles of TWs in human cognition.

A key property of TWs is their propagation direction. As a TW propagates, it reflects a moving wave of rhythmic neuronal activity that causes neurons across neighbouring cortical regions to activate sequentially according to the direction of wave propagation[8,22]. A TW's direction of propagation may thus indicate the sequence of activity across neighbouring cortical regions, with direction changes signalling a reorganization of the underlying neural connectivity and computation. In this way, separate neural processes and their associated behaviours might be reflected by TWs propagating in different directions, indicating the activation of different sequences of spatially organized neural assemblies[23,24]. For example, during perception, TWs may propagate in a posterior-to-anterior direction, which could indicate that neuronal activity flows from posterior sensory regions to the frontal lobe to support top-down processing[23–25]. Inversely, during internally driven behaviours controlled by the frontal lobe, TWs may propagate in

[1]Surgical Neurology Branch, NINDS, National Institutes of Health, Bethesda, MD, USA. [2]Amazon Corporation, Seattle, WA, USA. [3]Department of Mathematics, University of Pittsburgh, Pittsburgh, PA, USA. [4]Department of Biomedical Engineering, Columbia University, New York City, NY, USA. [5]Department of Neurological Surgery, Columbia University, New York City, NY, USA. e-mail: joshua.jacobs@columbia.edu

the reverse direction[26,27]. Thus, because TW propagation corresponds to the spatial structure of neuronal activity[8], the directional propagation of TWs can identify spatially organized neural assemblies and reveal the order in which cortical regions communicate to support different behaviours[22].

We hypothesized that changes in the directions of TWs provide a mechanism to flexibly organize large-scale brain activity to support different behavioural processes. We tested this hypothesis in the domain of human memory by measuring cortical TWs directly from neurosurgical patients performing an episodic memory task. Specifically, we considered whether TWs propagate in different directions during memory encoding and recall processes, given their reliance on externally and internally generated neural processes. We found that the brain's spontaneous TWs propagated in opposite directions during memory encoding and recall processes. These results demonstrate that different human cognitive processes are supported by large-scale patterns of oscillations that are TWs, with their propagation direction indicating the reorganization of cortical interactions to support behaviour.

Results

Measuring travelling waves in the human cortex

To examine how the direction and timing of TWs in the human brain relate to cognition, we examined electrocorticographic brain recordings from neurosurgical patients performing memory tasks. The dataset consists of recordings from 93 participants performing 222 sessions of an episodic memory task[28]. During this task, the participants showed neural oscillations at various frequencies across widespread brain regions, consistent with earlier work[28,29].

We analysed these multichannel recordings using spectral analysis and circular statistics to identify the neural oscillations that behaved as TWs and to assess their functional role[9,30]. A prerequisite for identifying a TW is that there must be an oscillation at the same frequency across a contiguous region of cortex. Thus, to identify TWs, in each patient we first identified the spatially contiguous clusters of five or more electrodes that simultaneously showed oscillations at similar frequencies, which we refer to as oscillation clusters. We then tested whether each oscillation cluster showed a TW by measuring whether the phase of these oscillations shifted progressively in space across electrodes within the cluster. To statistically test each cluster for a TW, we measured the instantaneous phase of the oscillation at each electrode and identified consistent phase gradients across neighbouring electrodes (Methods). A phase gradient across an oscillation cluster indicates that a TW is present because it means that the cycles of one oscillation are appearing with a progressive delay across neighbouring regions of cortex (Fig. 1). To ensure accurate measurements, we performed our analyses after excluding trials when it was challenging to accurately measure TW properties, such as when there was a possibility of spatial aliasing or low oscillatory power (Methods and Extended Data Figs. 1–3).

Consistent with earlier work[9,31], TWs were widespread in this dataset. We observed prominent oscillations and TWs across all brain lobes, in both hemispheres, at frequencies from 2 to 30 Hz. Overall, 73% of electrodes on the surface of the cortex were part of at least one oscillation cluster (Supplementary Table 1), and 83% of oscillation clusters exhibited significant TWs (Extended Data Fig. 4). TWs were prominent during the episodic memory tasks in 93 of the 160 participants that were implanted with surface electrodes (Supplementary Table 2). Figure 1a illustrates a TW at ~8.9 Hz that appeared in one trial of the episodic memory task in a patient's left temporal and frontal cortices. This oscillation was a TW because its individual cycles appeared with a progressive delay across neighbouring electrodes. Each cycle of this TW appeared first on inferior electrodes and later on anterior–superior electrodes, propagating with a phase velocity of ~1 m s^{-1} (Fig. 1b). We measured the propagation of TWs throughout the task using circular statistics to model the progression of phases across space (Fig. 1c and Methods). These phase gradients revealed the instantaneous direction, phase, phase velocity and strength (spatial consistency of the phase gradient). We then tested these features for links to behaviour.

To identify how TWs correlated with cognitive processes, we compared how TW features correlated with participants' performance in an episodic memory task. In this task, the participants learned and recalled sequences of words. After viewing each list, following a delay, they tried to freely verbally recall as many words as possible (Fig. 2a). On average, participants successfully recalled 27% of the viewed words. Because the participants remembered only a subset of the presented words in the task, we could test whether features of TWs differed according to whether a memory was successfully or unsuccessfully encoded.

Figure 2b–j shows data from an oscillation cluster in the temporal lobe of patient 34 with TWs at ~8.9 Hz during memory encoding and recall. In one trial when the participant viewed a word that they successfully encoded, the electrodes in this cluster showed a TW that propagated in a posterior-to-anterior direction (Fig. 2b–d). Inversely, later in that same list while the participant viewed a different word that they did not successfully encode, there was instead a TW propagating in the opposite, anterior-to-posterior direction (Fig. 2e–g; see also Supplementary Videos 1 and 2). Finally, during recall, before the participant spoke the recalled word, this oscillation cluster showed a TW propagating in an anterior-to-posterior direction (Fig. 2h–j). The direction of TWs on this cluster varied rapidly over time such that across trials TWs most often propagated along a predominant axis towards the anterior–superior direction or switched to the opposite direction. This pattern of results—in which the direction of TW propagation shifted according to the current memory process and performance—led us to systematically test the link between different memory processes and TW propagation direction.

Travelling waves propagate anteriorly during successful memory encoding

We examined the link between TW propagation direction and memory encoding by comparing the properties of the TWs that appeared during the presentations of words that were later remembered versus those that were forgotten. To illustrate the relation between TW direction and memory encoding, we first show results from a representative example participant in Fig. 3a for the same oscillation cluster shown above. Here, when the participant viewed words that they successfully encoded into memory, TWs in the alpha frequency band (8–12 Hz) propagated in a posterior-to-anterior direction ($t_{41} = 5.471$, $P = 0.003$, Rayleigh test). When the participant viewed words they did not successfully remember, the TWs here propagated bidirectionally, in a posterior-to-anterior direction on some trials and in an anterior-to-posterior direction on other trials (Fig. 3a(ii), middle). There was thus a significant difference in the distribution of directions of TW propagation between successful and unsuccessful encoding, with predominantly posterior-to-anterior propagation for successful memory encoding and bidirectional propagation for unsuccessful encoding (Fig. 3a(ii), $n_{\text{successful}} = 41$, $n_{\text{unsuccessful}} = 389$, $P < 0.001$, Kuiper circular two-sample test).

To measure the relation between propagation direction and memory encoding, we first identified whether an oscillation cluster showed bidirectional TW propagation across trials (Extended Data Figs. 5 and 6). We then measured the cluster's 'preferred encoding direction', which is the propagation direction that was most closely associated with successful memory encoding (Fig. 3a(iii) and Methods). We then labelled the time points of each trial according to whether the TWs were propagating in the cluster's preferred encoding or recall direction. We next tested, at each time point, the link between propagation direction and whether the participant successfully encoded the viewed word. Using this procedure, in patient 34 we found a reliable link between memory encoding and TW direction, which was strongest 305 ms after word presentation. At this time point, there was a 47% increase in propagation

https://doi.org/10.1038/s41562-024-01838-3

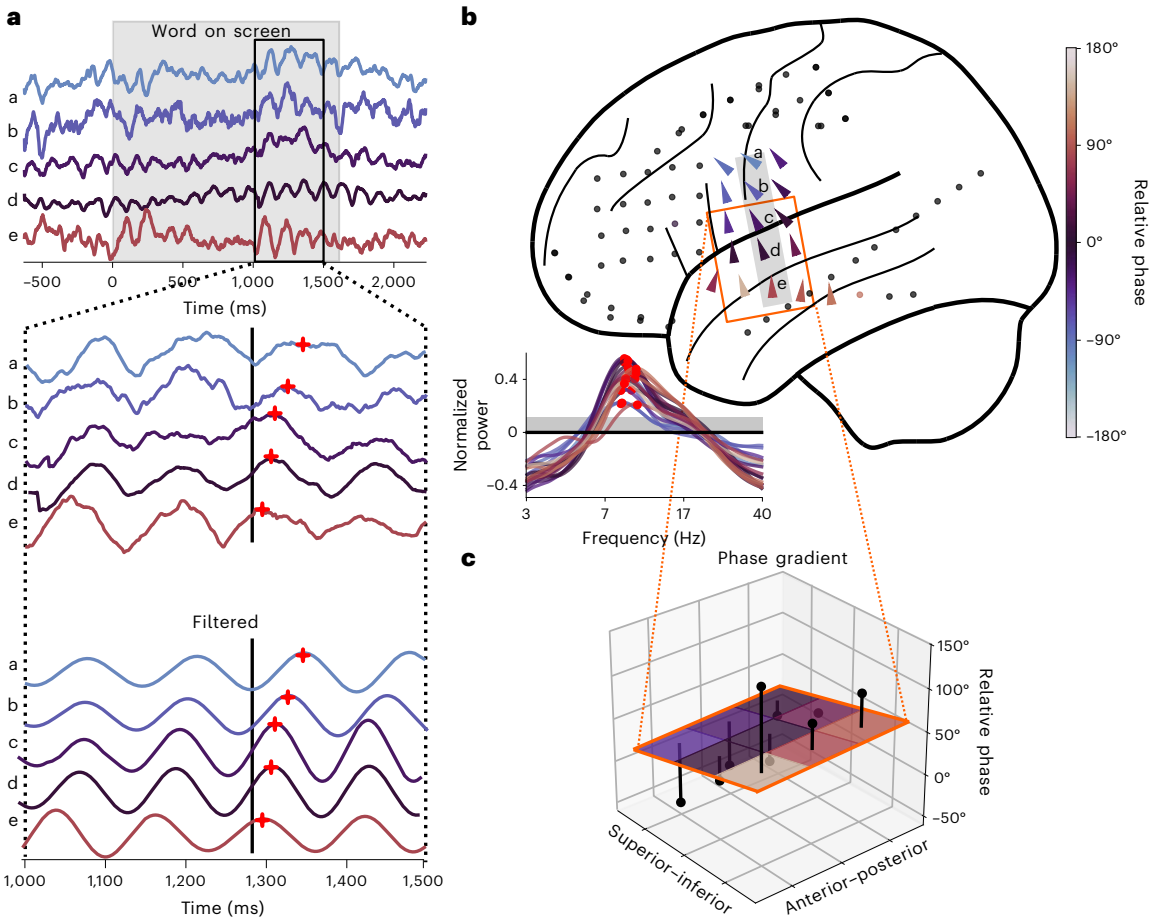

Fig. 1 | Example TW at 8.9 Hz in patient 34's left hemisphere. a, Recording from one trial of the memory task. Top, raw signal from five selected electrodes. Middle, expanded view of the signals from the top panel. Bottom, the signals from the middle panel after filtering at 8.9 ± 1.3 Hz. The colours indicate relative phase, measured at the time of the vertical black line. The red plus signs indicate peak phases of oscillations occurring sequentially across electrodes in **a**–**e**. **b**, Brain map indicating the TW in this trial[99,100]. The arrowheads indicate, for each electrode, the local propagation direction. The arrow colour indicates relative phase at the time indicated by the vertical black line in **a**. Normalized power spectra for each channel in the cluster were computed by removing the 1/*f* background signal from the power spectra. The red dots indicate the peak frequency of each electrode. **c**, Illustration of the circular–linear regression model for measuring the properties of TWs. This model estimates the spatial phase gradient at each electrode on the basis of the phases from the nearby electrodes' filtered signals. The black dots indicate the measured phase on each electrode, the plane indicates the model fit and the black lines between the dots and plane indicate residuals. The angle and slope of the fitted plane provide estimates of the TW's propagation direction and phase velocity, respectively.

towards the preferred encoding direction for successful versus unsuccessful encoding (Fig. 3a(iv); $P < 0.05$, permutation test, with two-sided cluster-based correction for multiple comparisons). Here, when this cluster showed a TW propagating in the preferred encoding direction (i.e., posterior-to-anterior), the odds that the participant would remember the word were 3.2× greater than in trials when a TW was propagating in the opposite direction (13% versus 4% respectively; $P < 0.01$, binomial test, Fig. 3a(iv)). Other participants also showed similar patterns of bidirectional propagation, with significantly better memory encoding when TWs propagated in the preferred encoding direction (Fig. 3b and Extended Data Fig. 7).

We next examined across the entire dataset (458 clusters from 93 patients) whether TW propagation direction correlated with successful memory encoding. Consistent with the examples described above, the preferred encoding directions for TWs on individual theta (2–8 Hz) and alpha (8–13 Hz) oscillation clusters were most often posterior-to-anterior, while beta (13–30 Hz) oscillation clusters' preferred encoding directions were more variable and differed between regions (Fig. 4a, top left; $t_{171} = 8.856$, $P < 0.001$, Rayleigh test; see also Extended Data Fig. 8). In contrast, propagation directions during unsuccessful memory encoding showed bidirectional distributions of propagation directions, which was driven by significant increases in propagation opposite to the preferred encoding direction (Fig. 4a, top right; all $n = 171$, $P < 0.001$, Kuiper circular test).

We found that the propagation of theta- and alpha-band TWs correlated with memory encoding at distinct latencies during word presentation. The odds of successful memory encoding increased by ~1.7× if theta TWs at ~250–800 ms after word presentation were propagating in the preferred encoding direction (Fig. 4b, left; $P < 0.001$, two-sided cluster-based permutation tests; see also Supplementary. Fig. 1 and Methods). Similarly, the odds of successful memory encoding increased by ~1.4× if there was an alpha-band TW propagating in the preferred direction—this effect began 72 ms before word presentation ($P < 0.05$, two-sided cluster-based permutation test; Fig. 4b, right).

Overall, it was common for clusters to exhibit TWs that switched between propagating in two opposite directions over time, thus showing bidirectional propagation (57% of all clusters; Extended Data Figs. 5 and 6a and Methods). Of these clusters that showed bidirectional propagation patterns, 68% had one particular direction that was significantly associated with successful memory encoding (all $P < 0.05$, binomial tests corrected for false discovery rate (FDR); Methods and Supplementary Table 1). This indicates that the phenomenon of bidirectional TWs was

https://doi.org/10.1038/s41562-024-01838-3

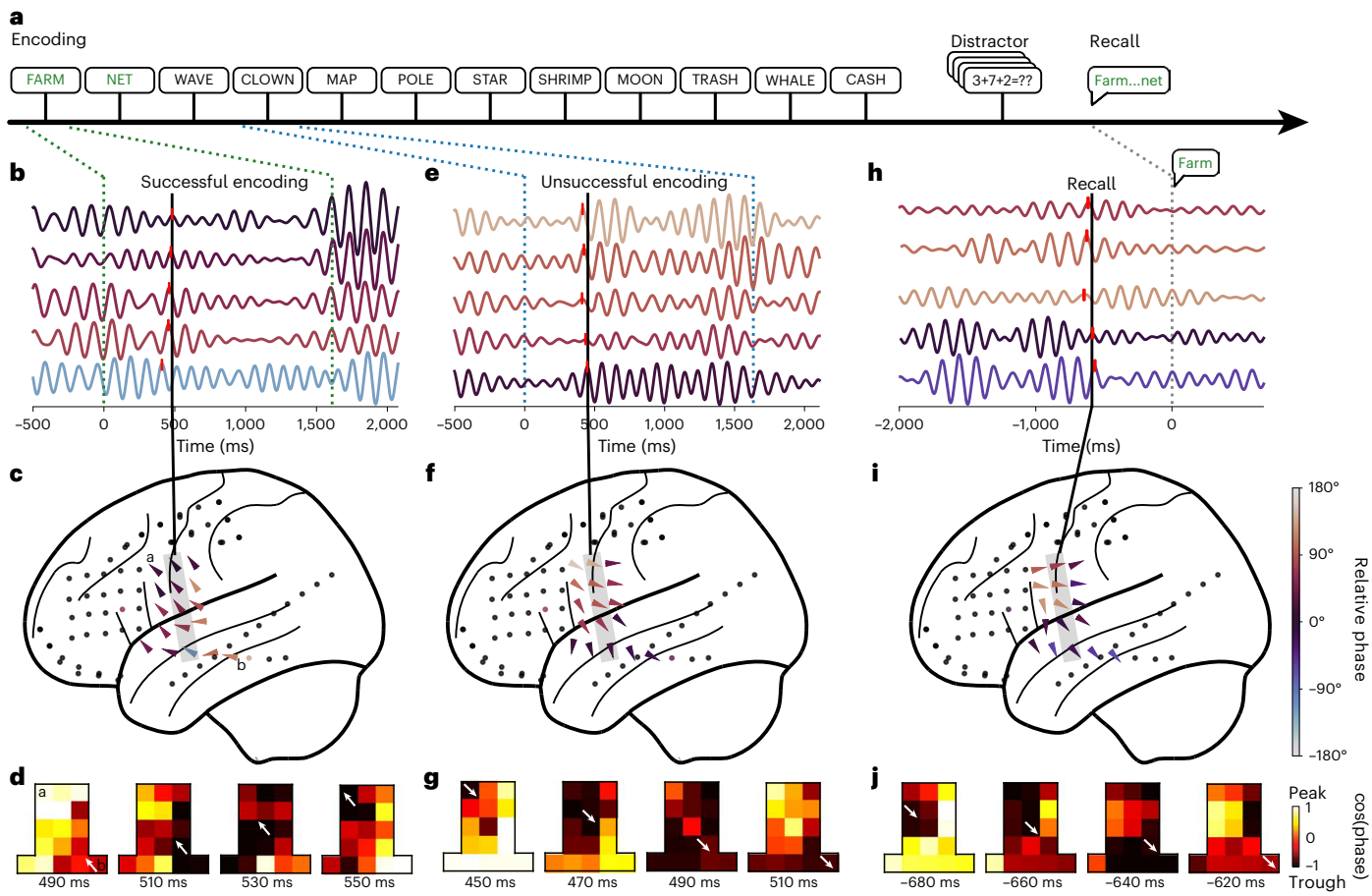

Fig. 2 | Changes in TW direction across memory encoding and recall. **a**, Timeline of one trial of the verbal memory task for patient 34. Words in green were successfully encoded; black words were forgotten. **b**, Recordings on five electrodes in one trial while the participant successfully encoded the word 'FARM'. The signals were filtered at 4.5 Hz, and the electrodes are ordered from anterior (top) to posterior (bottom). The red ticks indicate peaks of one oscillation cycle, which illustrates an example TW because there was a progressive shift in the timing of these peaks across electrodes. **c**, Brain map with arrowheads showing the direction of TW propagation for the time point labelled with the black line in **b**. **d**, Topography of this TW's propagation across a 3 × 6 array of electrodes within the oscillation cluster from **c** (the labels a and b indicate the corresponding electrodes). Each panel indicates the topography of instantaneous phase at one of four sequential time points. The white arrows at the troughs of oscillations indicate the TW propagation direction. **e**–**g**, A representative TW measured during unsuccessful memory encoding where the participant viewed the word 'CLOWN', with plots analogous to **b**–**d**. **h**–**j**, A representative TW measured prior to the recall of the word 'FARM'.

generally related to higher-level cognition and memory (Extended Data Fig. 9 and Supplementary Fig. 2). This link between memory performance and the direction of TW propagation was specifically present at significant levels in the theta (2–8 Hz) and alpha bands (8–13 Hz) in the frontal and temporal lobes and in beta bands in the frontal lobe (Extended Data Figs. 8 and 9 and Supplementary Fig. 3; all $P < 0.05$, binomial tests against 0). We found that clusters with bidirectional TWs were smaller than clusters with unidirectional patterns (Kruskal–Wallis, $h = 11.8$, $P = 0.002$), which may indicate that spontaneous wave direction changes occur more locally than globally across the cortex.

We considered the possibility that this correlation with memory could be more strongly driven by other features of TWs, such as the power of ongoing oscillations, rather than propagation direction specifically. However, we did not find a significant relation between memory encoding and the power of ongoing oscillations or with the phase velocity or strength of TWs (all $P > 0.05$; Supplementary Table 3 and Extended Data Fig. 2). Our results thus indicate that the link between TWs and memory encoding was specific to the direction of propagation. We also considered whether the presence of waves may facilitate successful encoding; however, we did not find a significant relation between recall rates and the presence of a TW during encoding (for all regions and oscillatory ranges, $P > 0.05$, paired t-tests), thus indicating that the direction rather than presence of a TW is most important for predicting memory.

Travelling waves propagate posteriorly during memory recall

Immediately before the participant verbally recalls each word, they are actively searching their memory[32,33]. We hypothesized that a different pattern of TWs would be present during this search period. To examine the propagation of TWs during memory recall, we examined the same cluster of electrodes (example participant 34) during the period prior to the patient speaking aloud the remembered item (Fig. 3a(i)–(v)). Here, rather than the posterior-to-anterior propagation that appeared during encoding, TWs tended to propagate in the reverse, anterior-to-posterior direction (Fig. 3a(ii), right), which we refer to as the cluster's preferred recall direction. This cluster's propagation direction during recall was reliably different compared to successful encoding (all $n = 41$, $P < 0.05$, Kuiper circular test) and was strongest 865 ms prior to word recall (Fig. 3a(v)). The direction of TW propagation on this cluster thus correlated with the current memory process, switching directions between successful encoding and recall. Similar patterns were present in other participants (Fig. 3b and Extended Data Fig. 7).

https://doi.org/10.1038/s41562-024-01838-3

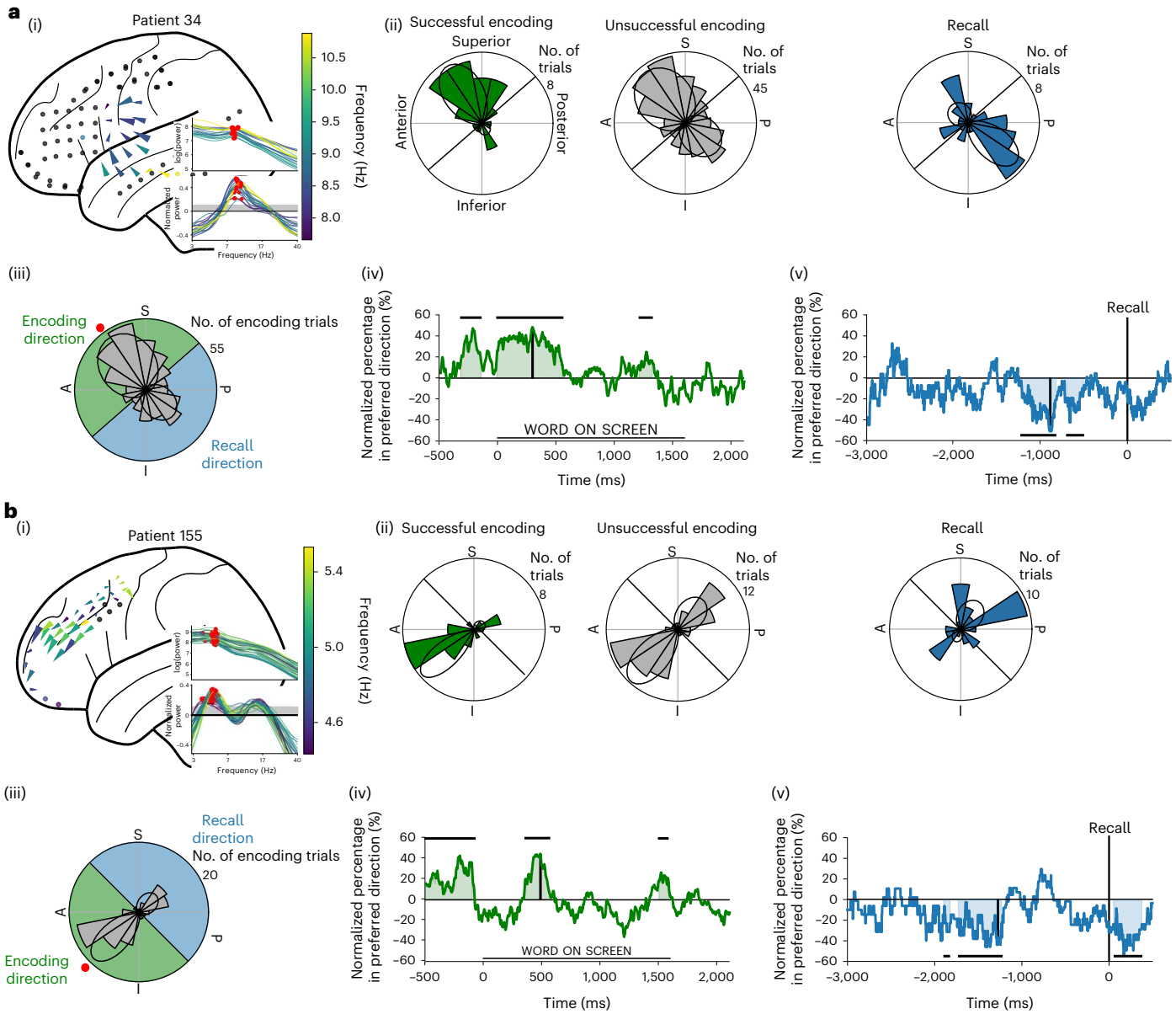

Fig. 3 | Example participants where TWs varied in propagation direction with memory processing. a, (i) Brain map showing the mean direction and frequencies of TWs measured in the left hemisphere of patient 34 during successful memory encoding. The arrowheads indicate the mean propagation direction for each electrode averaged across trials. Arrowhead size indicates directional consistency. Raw and normalized power spectra for each channel in the cluster were computed by removing the 1/*f* background signal from the power spectra. (ii) Distribution of TW propagation directions across trials, averaged across the electrodes from **a**, during successful memory encoding (left), unsuccessful encoding (middle) and recall (right). Predominant directional clusters are indicated by black ellipses (Methods). (iii) Propagation directions of TWs across all encoding trials. The preferred encoding direction is marked with a red dot; green and blue shading indicate the range of angles labelled as preferred encoding and preferred recall directions, respectively. (iv) Time course of the link between TW propagation direction and memory encoding. The line indicates the difference in the percentages of TWs moving in the preferred encoding direction between trials with successful memory encoding compared with unsuccessful encoding. The vertical black line indicates the time of the maximal difference, which corresponds to (i)–(iii). The horizontal black lines indicate time points when directional shifts are statistically significant ($t_1 > 2.5$, $P < 0.05$, two-sided cluster-based permutation test). Positive values (shaded green) indicate a greater percentage of waves propagating in the anterior–superior direction relative to the baseline. (v) The link between TW propagation direction and memory recall. The line indicates the normalized percentage of trials propagating in the preferred encoding direction prior to memory recall at time 0. The values are normalized relative to the cluster's baseline period. Negative values (shaded blue) indicate a greater percentage of waves propagating in the posterior–inferior direction relative to the baseline. The vertical black line indicates the time point of the greatest propagation shift away from the preferred encoding direction (which matches the right panel of (ii)). The horizontal black lines indicate significant time points measured by binomial tests. **b**, Same as (i)–(v) for patient 155.

Across all participants, TWs on 52% of the oscillation clusters with bidirectional propagation exhibited a significant pre-recall direction shift. This usually involved increased anterior-to-posterior propagation prior to recall (Fig. 4a, bottom, $t_{171} = 5.952$, $P = 0.002$, Rayleigh test). Prior to recall, there was a significant shift away from the preferred encoding direction for theta- (16%) and alpha-band TWs (17%), particularly in the frontal and temporal lobes (Fig. 4c, two-sided cluster-based permutation testing one sample against zero; Extended

https://doi.org/10.1038/s41562-024-01838-3

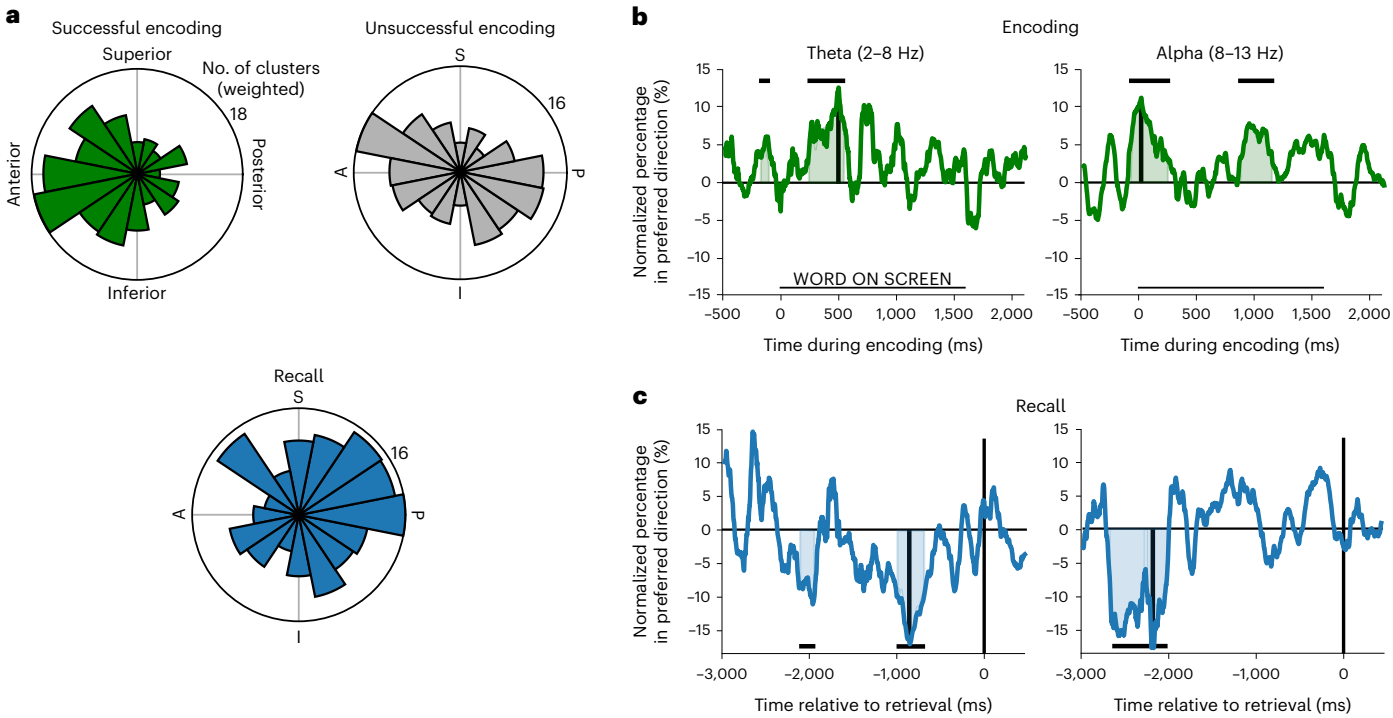

Fig. 4 | Population analysis of TW direction shifts during memory encoding and recall. a, Distribution of clusters' predominant propagation directions for all theta and alpha TWs measured on oscillation clusters primarily located in the frontal, temporal and parietal/occipital regions during memory encoding and recall at the time point of maximal memory-related effects. **b**, Time courses of TW directional shifts during successful and unsuccessful memory encoding averaged across all theta (left) and alpha (right) TWs measured on oscillation clusters primarily located in the frontal, temporal and parietal/occipital regions. The black vertical lines indicate the time point of peak propagation in the preferred direction. The horizontal black lines and green shading indicate the timing of statistical significance at $P < 0.05$ using two-sided cluster-based permutation testing, with the position at the top or bottom of the plot indicating the direction of the effect. **c**, Time courses of TW directional shifts prior to memory recall averaged across all theta (left) and alpha (right) TWs measured on oscillation clusters primarily located in the frontal, temporal and parietal/occipital regions. The black vertical lines indicate times of maximal propagation away from the preferred encoding direction. The horizontal black lines and blue shading indicate the timing of statistical signifiance.

Data Fig. 9, binomial tests, all $P < 0.05$, FDR multiple comparisons corrected; Supplementary Table 1, binomial tests, all $P < 0.05$, FDR multiple comparisons corrected). Memory recall is thus associated with TWs propagating in an anterior-to-posterior direction, the opposite of the direction for memory encoding, with this effect being most prominent in the theta-band TWs in the frontal and temporal lobes and in the alpha-band TWs in the temporal, parietal and occipital lobes.

Discussion

A persistent question over the past few decades has been how widespread areas of the brain organize their interactions to support different behaviours. TWs provide one answer to this question by propagating in particular directions across the brain to coordinate neuronal activity with high temporal precision. Here we found that the TW direction correlates with memory encoding and recall, which suggests that propagating neural oscillations support cognition by organizing the spatiotemporal structure of neural activity.

Prior studies have shown that the theta and alpha oscillations that comprise TWs are phase locked to neuronal spiking and high-frequency oscillations via the phenomenon of phase–amplitude coupling[8,34,35]. With our findings, this suggests that the propagation of theta and alpha oscillations across the brain as TWs indicates when and where the brain is exhibiting discrete pulses, or 'packets', of neuronal activity moving across the cortex[36,37]. The propagation direction of theta and alpha TWs may thus reveal the sequence in which neural representations are communicated across brain regions. These findings have fundamental implications for explaining how different brain regions represent information and interact to support behaviour[38]. For information to move from one cortical region to the next, discrete packets of spiking activity may propagate between contiguous regions coordinated by the phase of ongoing TWs[39,40].

The phase velocities of the TWs that we report are generally consistent with axonal conduction velocities in unmyelinated axons, which are common in superficial layers of the cortex[1,41,42]. Although in some cases TWs appear to propagate with slower phase velocities than axonal conduction speeds, this may be expected because theoretical models of TWs suggest that the propagation speed relies on many factors beyond axonal conduction, including the local intrinsic oscillation frequency at each site and coupling between oscillators. Thus, the phase velocity of TWs may not directly reflect axonal conduction speed but rather the phase lags in the oscillations that are due to the heterogeneity of intrinsic oscillation frequencies. It is likely that the propagation of these oscillations relies on a combination of synaptic and non-synaptic electrical activity as well as the coupling function between oscillators, which is reflected in the range of phase velocities we observe[1,43].

A key aspect of our results is identifying a link between distinct directions of TW propagation and separate functional processes, particularly memory encoding and recall. In conjunction with earlier research[24,44–46], this suggests that a fundamental way in which the brain's functional connectivity transiently reorganizes is by changing the directional interactions between different brain regions. Posterior-to-anterior TWs were associated with successful memory encoding and anterior-to-posterior TWs were associated with memory recall (Extended Data Fig. 10), suggesting that forming new episodic memories involves the flow of neural activity from posterior regions into the frontal lobe[47]. However, memory recall involves the flow of

neural activity in the opposite direction from the frontal lobe, where internally generated context is most strongly represented[27,48,49]. Our finding that TWs reverse direction prior to recall is particularly important because unlike prior studies that have shown shifts in propagation direction when comparing the presence and absence of visual stimuli[24,44], our study demonstrates anterior-to-posterior TWs during an active cognitive process of searching one's memory for previously encoded words. While the differences in TW direction between successful and unsuccessful encoding may be influenced by perceptual processing of the presented word and whether it was represented and transferred into memory, it is unlikely that the directions of TWs prior to recall in the absence of visual cues were modulated by perceptual processing. Our findings thus provide substantial advances in linking TW direction to the process of memory retrieval.

One more general possibility is that posterior-to-anterior TWs correspond to feedforward processing while anterior-to-posterior TWs correspond to feedback processing[50–54]. This interpretation builds on earlier work showing that different patterns of neuronal oscillations modulate feedforward networks during visual perception[52,55] and feedback processing during top-down control and prediction[26]. Consistent with our results, there is also other evidence of neural activity changing direction for specific functional states[24,44,56–60], thus suggesting that our results are part of a broader phenomenon.

An important question going forward is to understand the mechanisms underlying cortical TWs and, in particular, how TW propagation may shift to support different behaviours. Some work suggests that TWs in the cortex are driven by underlying corticothalamic networks[61,62] (but see Halgren et al.[63]). Thus, one potential mechanism by which the direction of TW propagation could change is by local increases in excitation at certain thalamic subregions. This excitation could accelerate the frequency of cortical oscillations[19] and alter TW propagation direction, as predicted by coupled-oscillator models of TWs[1,9,64]. Computational models of TWs could thus be useful for assessing the potential mechanisms underlying memory-related direction shifts[2,39]. Future work may also use direct electrical stimulation to causally manipulate characteristics of spontaneous TWs to distinguish functional mechanisms from epiphenomena.

A TW propagating in a particular direction may indicate that a region is uniquely engaged in a particular functional process. However, a further possibility is that the neural networks in individual regions simultaneously support multiple directionally organized processes, such as concurrent feedback and feedforward processing[51]. Following this view, the propagation direction of TWs at each moment may be informative about the current weighting, or attention, given to each process. Consistent with this idea, prior work has demonstrated a link between the amplitude of neuronal oscillations and the attention given to specific neuronal representations[65,66]. In the context of our results, the presence of posterior-to-anterior TWs during successful memory encoding may indicate that the brain is currently attending to feedforward processing to represent the current stimulus and transfer it to memory (Extended Data Fig. 10). Inversely, the bidirectional patterns during unsuccessful encoding may indicate that feedforward processes were attended more weakly[39,67]. Following this logic, the increases in anterior-to-posterior TWs before recall may correlate with top-down processing related to memory search[48,49]. We additionally detected a small subset of clusters with multidirectional patterns, with three or more main directions, which may be interesting to explore in future work.

Our findings suggest that many TWs relevant to behaviour are endogenous and ongoing in the brain, rather than being evoked by task events. This is most notable for alpha-band TWs, whose direction correlated with performance before word presentation during encoding, indicating that the oscillations were present prior to stimulus onset. This heightened relevance of alpha-band TWs prior to encoding indicates a distinct role in priming relevant brain regions to be in an optimal state for successfully encoding an item into memory[68–73]. In contrast to our alpha-band results at early time points, it is notable that we found that theta-band TWs correlated with memory at later time points, because this suggests that theta TWs have a fundamentally different functional role[60,74–76].

It might be considered surprising that some of our results were not observed previously, given that human brain oscillations have been measured for decades. It is possible that many previous studies reporting directional patterns in a range of behaviours were actually related to TWs[75,77–79]. Our results relied on new analytical methods, which may have been essential for our findings. In particular, one challenging aspect of measuring TWs in humans is that there is substantial variation in oscillation frequencies and propagation directions across participants and brain regions. Our analysis framework accommodated this diversity by measuring each participant's TWs in a customized manner rather than assuming identical propagation and frequencies across all participants. The fact that we observed substantial variability across individuals emphasizes the importance of analysing human brain data in a manner that accounts for electrophysiological differences between participants[80–82]. Additionally, we detected many oscillation clusters with contacts crossing sulci and gyri. We consider such contacts to be part of the same oscillation cluster. Since anatomical geometries probably impact spatiotemporal neural dynamics[83], future work may explore changes in directional patterns across sulci and gyri using an inflated brain surface of the cortex model[84]. In light of the analytical challenges of measuring TWs in humans and the hints of similar patterns in prior literature, TWs may actually have a much broader role in behaviour and cognition than previously appreciated.

TWs may be useful for practical purposes, beyond fundamental research. Our findings have translational and clinical applications because they suggest that measuring TWs could improve our ability to interface with the brain and diagnose neurological disorders. For brain–computer interfacing, TWs might be a useful neural signal for more effectively decoding the brain's current state. In particular, our direction results indicate that measuring TW propagation can indicate whether the current brain state is well suited for memory encoding. Going forward, it may be possible to use TWs to measure more advanced aspects of cognition, perhaps with the use of improved recording methods, including high-density neural recording arrays[44,85,86], as well as non-invasive methods[16,87,88]. Furthermore, TWs could provide biomarkers for identifying neurological disorders related to abnormal neural connectivity such as autism[89] or epilepsy[90]. Characterizing the directional propagation of TWs thus holds the potential for new approaches to brain–computer interfacing and disease diagnosis by revealing when the brain's current communication state is abnormal. TWs may also be useful for guiding the clinical use of brain stimulation, by providing a target biomarker that reflects neural connectivity.

Methods

Participants

The 93 participants who contributed data to our study by performing an episodic memory task were pharmacoresistant epilepsy patients surgically implanted with grids and strips of electrodes on the surface of their cortex for the purpose of identifying epileptogenic regions. The patients' clinical teams determined electrode placement to best monitor each patient's epilepsy. Data for the episodic memory task were collected at eight hospitals: Thomas Jefferson University Hospital (Philadelphia, Pennsylvania), University of Texas Southwestern Medical Center (Dallas, Texas), Emory University Hospital (Atlanta, Georgia), Dartmouth–Hitchcock Medical Center (Lebanon, New Hampshire), Hospital of the University of Pennsylvania (Philadelphia, Pennsylvania), Mayo Clinic (Rochester, Minnesota), National Institutes of Health (Bethesda, Maryland) and Columbia University Hospital (New York, New York). Following approved institutional review board

experimental protocols at each hospital, all participants provided informed written consent.

Verbal memory task

In the episodic memory task, the participants performed a verbal free-recall paradigm[28], in which they were asked to memorize a list of 12 words sequentially presented as text on the computer screen. Figure 2a presents the timeline of an example list. Each word was presented for 1,600 ms, followed by a blank screen for 750–1,000 ms. The lists consisted of high-frequency nouns (http://memory.psych.upenn.edu/Word_Pools). After the list, the participants were presented with a 20 s math distractor task prior to recall. During recall, the participants were given 30 s to verbally recall the words in any order. We recorded the verbal responses on a microphone and then manually scored the recordings after the task.

Participants performed one or both versions of this task that differed in the semantic categorization of the word lists. One version of the task selected 300 words from the Toronto word pool with intermediate recall performance. Lists of 12 words were constructed such that the mean pairwise semantic similarity within list was relatively constant across lists. For the categorized version of the free-recall task, the words were selected from semantic categories rated by users using Amazon Mechanical Turk and sequentially presented as categorical pairs of words from the same category. Each list consisted of four words drawn from each of the three categories such that two pairs drawn from the same semantic category were never presented consecutively.

Electrocorticographic brain recordings and referencing

During the tasks, data were recorded at 500, 1,000 or 1,600 Hz using a clinical intracranial electroencephalographic recording system at each hospital (Nihon Kohden EEG-1200, Natus XLTek EMU 128, Natus Quantum EEG or Grass Aura-LTM64 systems). Subdural grid and strip electrodes had a distance of 10 mm between contacts. Each electrode's signal was initially referenced to a common contact placed intracranially, on the scalp or on the mastoid process. We filtered electrical line noise using a fourth-order Butterworth notch filter at 58–62 Hz. We identified the location of each electrode by co-registering a structural magnetic resonance image taken prior to surgery with a computed tomography image after the electrodes were surgically implanted to compute electrode locations in standardized Talairach coordinates[91].

Identifying TWs

We defined a TW as a single oscillation at one frequency that appears across a region of cortex with a progressive phase shift. To identify TWs in our data, we first used an algorithm to identify spatially clustered groups of electrodes, or oscillation clusters, that showed oscillations at approximately the same frequency. We then measured whether the phase across these clusters showed the progressive phase shift that characterizes TWs[9,92]. To find these oscillation clusters, we first identified groups of at least five neighbouring surface electrodes that showed narrowband oscillations within a 2 Hz window, while being within 25 mm of at least one other electrode with a similar frequency peak. We found the frequencies of these narrowband oscillations on each electrode individually by identifying peaks in the normalized power spectrum, which we measured at 200 frequencies logarithmically spaced from 2 to 40 Hz using Morlet wavelets. We removed the $1/f$ background signal and identified peaks that were local maxima that were at least one standard deviation above the mean.

Next, building on methods from Zhang et al.[9], we identified TWs by identifying local plane waves across the electrodes in each oscillation cluster using a circular–linear regression model[30]. To measure the instantaneous phase at each electrode, we first applied a Butterworth filter to each electrode's signal on each trial, with a filter bandwidth that extended ±15% around the electrode's mean narrowband frequency. We then measured the instantaneous phase of each electrode's filtered signal using the Hilbert transform. At each time point, we converted the phase at each electrode to a relative phase shift by subtracting the mean phase of the oscillations measured across all electrodes in the oscillation cluster. We used circular statistics to manipulate all phase values with the Python library PyCircStat toolbox[93].

Measuring local propagation direction

Having computed the relative phase shift on each electrode at each time point, we next tested for spatial propagation of the oscillation across the cluster. Whereas our earlier work performed this task by fitting one propagation direction for the entire cluster[9], here we separately fit the direction for each electrode individually. By allowing each electrode to have its own propagation direction, this method has improved sensitivity to TWs with non-planar and complex propagation patterns, as well as to TWs that were present at only a subset of the electrodes in the cluster, which could otherwise not be detected reliably with a singular phase gradient across the entire oscillation cluster. Using this method, we were able to able to capture complex, non-planar patterns where a singular phase gradient for the entire cluster would not suffice (see example clusters in Extended Data Fig. 7).

We fit the circular–linear model for each electrode individually, on the basis of the phase gradient measured on the nearby electrodes (within 25 mm) in the cluster. We fit this model only for electrodes with at least three nearby contacts. This procedure measured the features of the TW propagation around each electrode by quantifying the propagation direction (an angle $\alpha \in [0°, 360°]$) and the spatial frequency ($\xi \in [0° \text{ mm}^{-1}, 18° \text{ mm}^{-1}]$). To compute these parameters that describe the local TW at each electrode i and time point, we fit the equation

$$\hat{\theta}_i = (ax_i + by_i + \vartheta) \bmod 360°$$

where $a = \xi\cos(\alpha)$, $b = \xi\sin(\alpha)$, and x and y are the electrode's spatial coordinates. Following earlier work[9,30], we used a grid search to optimize the values for a and b. This grid search identified the propagation direction and spatial frequency for each TW by minimizing the difference between the predicted phase ($\hat{\theta}$) and actual (θ) phase values across the nearby electrodes. Phase velocity, or the distance a cycle of an oscillation travels over time, was derived from spatial frequency and oscillation frequency. We measured the statistical reliability of each model fit by computing the circular correlation coefficient between the predicted and actual phases and then adjusting for the number of fitted parameters and data points (ρ_{adj})[9,94].

Applying this model to each electrode individually, we then used two criteria to label an electrode cluster as exhibiting a significant TW on a given trial. First, we required that each cluster have a reliable phase gradient at the group level, as determined by averaging the adjusted correlation coefficient from all the electrodes in the cluster and ensuring it was above 0.2 (that is, $\rho^2_{\text{adj}} \geq 0.2$). Second, we ensured that the mean power spectrum across all electrodes exhibited a robust narrowband peak. See Extended Data Fig. 3 for examples of trials without significant TWs. On the basis of these criteria, we included in our analyses oscillation clusters that had reliable TWs on at least 30 encoding trials and at least 10 successful encoding trials with TWs.

Controlling for measurement inaccuracy from spatial aliasing

The 1 cm distance between cortical grid and strip electrodes with which we recorded TWs leads to the theoretical possibility of incorrectly estimating the directions and phase velocities of TWs due to inadequate spatial sampling (Extended Data Fig. 1a). Spatial aliasing, the inadequate sampling of neural oscillations in space across the cortex, may occur when half the spatial wavelength of a propagating oscillation is less than the distance between electrodes. For 1 cm electrode spacing, this occurs when oscillations have a spatial frequency of greater than $\pi/2$ cycles per centimetre, which is most common when high-frequency oscillations propagate at slow phase velocities (Extended Data Fig. 1b).

When spatial sampling is inadequate, it is theoretically possible for the phases measured on adjacent electrodes to not reflect the same cycle of a travelling oscillation but rather be from the previous or next cycles (Extended Data Fig. 1a, middle). In these cases, the correct propagation direction can be determined with complete certainty only with greater spatial sampling or higher-density electrode grids and strips (Extended Data Fig. 1a, right).

To control for this issue, we implemented a framework to exclude trials that could be susceptible to spatial aliasing (Extended Data Fig. 1c–f). To identify these trials, we used a complementary method for measuring wave propagation based on measuring the time-lagged cross correlation between the raw signals measured on adjacent neighbouring electrodes (Extended Data Fig. 1c,d). This method is less sensitive to aliasing because it can take advantage of a range of frequencies as well as non-sinusoidal aspects of the signal besides phase to measure propagation. If the time lag of maximum coupling measured from cross correlation aligned with the phase differences measured from narrowband oscillations, we could proceed in measuring TW direction with certainty that spatial aliasing was not occurring (Extended Data Fig. 1e). When time-lagged cross correlation did not align with phase measurements, particularly if the time lag corresponded with the duration of one wavelength of the oscillation frequency in the positive or negative direction, it is possible that the propagation direction measured with phase differences was inaccurate due to spatial aliasing (Extended Data Fig. 1f). When excluding these trials across all oscillation clusters, we found that 83% of trials were not susceptible to spatial aliasing. We did not find evidence that smaller oscillation clusters may be more susceptible to spatial aliasing (Spearman's $\rho = 0.22$, $P = 0.99$, one-tailed test of negative correlation). We thus included in our study only the trials where the measured wave propagation was consistent between the time-lagged cross correlation and phase methods.

We performed a simulation with constructed TWs where we knew the ground-truth propagation direction to measure the impact of aliasing on the measurements of TW direction with actual human brain signals. Because human brain signals are not perfectly sinusoidal, we inferred that aliasing would be less likely with actual human brain signals (Extended Data Fig. 1h–j). We found that the propagation direction of only 56% of beta oscillation trials could be measured accurately with perfect sine waves; however, when measuring this percentage using real human brain signals, 73% of trials could be measured accurately (Extended Data Fig. 1h,i), thus indicating that aliasing is less of a concern with human brain waves than with sine waves. Nonetheless, to be sure that aliasing did not meaningfully impact our results, we applied an additional procedure where we removed all trials that were potentially susceptible to spatial aliasing as determined with the time-domain method described above. Our simulation shows that excluding these 17% of trials across the dataset increased the accuracy of direction measurement to 99% (Extended Data Fig. 1j).

Categorization of cluster directionality

Across oscillation clusters, we found TWs that exhibited wide-ranging propagation patterns, including unimodal, bimodal and multimodal distributions of directions. To characterize these diverse patterns, we designed a method to quantify multimodal directional distributions rather than only unimodal directional distributions.

To characterize these varying types of propagation patterns, we fit a mixture of von Mises distributions[30] (the circular analogue to Gaussian distributions) to the distribution of propagation directions from all encoding trials (Extended Data Fig. 5). We fit this pattern using a non-parametric model-fitting procedure for circular data, which modelled the overall direction distribution as a mixture of multiple von Mises distributions, each with a different angle and magnitude. In this model, each individual fitted von Mises distribution reflects one particular direction in which the TWs on the cluster frequently propagate. Distributions fitted with more than one von Mises distribution thus showed multiple distinct propagation directions. We used an iterative method to determine the best-fitting mixture of von Mises curves, as the sum of the minimum number of von Mises curves (each centred at a different direction) that would fit at least 99% of the variance in the original distribution of propagation directions[57,95]. We then labelled each cluster as showing unidirectional or bidirectional propagation on the basis of the directions and magnitudes of the mixture of individual fitted von Mises curves. If at least 80% of a cluster's propagation directions were fit by a single von Mises curve, then we labelled it as showing unidirectional propagation. Likewise, we labelled a cluster as bidirectional if two von Mises distributions (each representing 20–80% of TW directions) were required to capture its propagation distribution. We labelled a cluster as showing non-directional TW propagation if it exhibited no consistent direction over trials (Rayleigh test, $P > 0.05$) or if its propagation patterns could be accurately fit only by a mixture of three or more von Mises distributions (this was required in 6% of all clusters). We measured some oscillation clusters in the 2–3 Hz range, and there seemed to be no distinct functional role between these lower-frequency clusters and theta–alpha-band clusters; thus, we grouped them in with theta-band clusters.

Determining a cluster's preferred propagation direction

Next, for the clusters with bidirectional TW propagation, we tested whether one of the two predominant directions was preferred for memory encoding. To do this, we followed the earlier fitting approach but applied it just to the trials where memory encoding was successful. We labelled the cluster's preferred direction as the angle of the von Mises distribution from the overall model fit that was closest to the most prominent propagation direction fit to the successful encoding trials. We determined the preferred angle from the model fit to all trials because this larger dataset provided more precision in categorizing propagation directions as either towards or away from the preferred encoding direction. On the basis of these calculations, we then used the fitted angles to label whether a TW on each individual trial propagated towards or away from the cluster's preferred encoding direction (Fig. 3c).

Calculating the relation between TW direction and memory

To measure the timing of the link between a cluster's propagation direction and memory encoding, we measured the prevalence of TWs moving towards or away from the preferred encoding direction at different time offsets relative to stimulus presentation. We performed this calculation separately for trials where the word was successfully encoded and for trials where it was unsuccessfully encoded. We determined the cluster's preferred propagation direction on the basis of the time point with the strongest difference in propagation direction between successful and unsuccessful memory encoding, and we then recalculated the entire time course (2.6 s starting and ending 0.5 s before and after word presentation) of difference scores for each cluster on the basis of that identified preferred encoding direction. We used permutation tests to determine the statistical significance of the relation between TW propagation and memory encoding (see below).

For memory recall, we used a related method to identify the behavioural role of TW direction. At each time point relative to word recall, we calculated the percentage of trials with TWs propagating in the cluster's preferred encoding direction, as determined during encoding. We calculated this for the 3 s prior to word recall or from the time of the previously spoken word if within 3 s of each other. Because we wanted to measure task-related changes, and individual clusters showed variability in their overall level of TW propagation, we performed a baseline normalization for each cluster. For each cluster, we normalized the observed percentage of TWs propagating in the preferred encoding direction relative to the cluster's non-memory baseline. This baseline included task periods with no stimuli on screen, including intertrial intervals.

To examine whether TWs moved in specific anatomical directions for particular memory processes (Fig. 4), across all oscillation clusters

we computed a weighted distribution of the anatomical directions of TW propagation for each memory process. The weighting for each cluster's directions was determined from the percentage of individual trials that was captured by that direction's underlying von Mises curve. This method ensures that the shape of the overall circular histogram is representative of the population's proportion of waves propagating in each direction.

Statistical procedures

We used a cluster-based permutation procedure to assess whether the directional patterns that distinguished successful versus unsuccessful memory encoding were statistically reliable[96]. For each oscillation cluster, we generated 100 random surrogate datasets by shuffling the labels that indicated whether each item presentation was successfully remembered or forgotten. Then, for each random surrogate dataset, we recomputed the statistical procedure, thus providing a distribution of surrogate test statistics. We tested the significance of the original directional difference score by comparing its test statistic with the distribution of surrogate test statistics. This procedure adjusts for multiple comparisons across time points because we summed the significant test statistics for each trial across all potentially significant clusters of contiguous time points that were individually significant at $P < 0.05$ (ref. 97).

We performed a similar procedure to assess significance for recall, except here we tested the statistical significance of pre-recall direction shifts using two-sided binomial tests. The tests compared the prevalence of preferred encoding and preferred recall propagation at each time point before recall relative to the level in the baseline period for that cluster, correcting for multiple comparisons with the FDR procedure[98].

To test the reliability of memory-related direction changes across all participants during both encoding and recall, we used a non-parametric two-sided cluster-based permutation test of one sample against zero[96]. This method identified contiguous time periods relative to the timing of behavioural events where TWs showed reliable increases or decreases in propagation towards or away from their preferred encoding direction. This procedure assessed significance at the group level for consecutive temporal intervals by comparing the results with those found from applying the same procedure to 1,000 surrogate values from random shuffling, with correction for multiple comparisons by calculating the test statistic using the maximum value of the cluster-level summed statistics.

Reporting summary

Further information on research design is available in the Nature Portfolio Reporting Summary linked to this article.

Data availability

The raw electrophysiological data used in this study are available upon request at https://memory.psych.upenn.edu/Data_Request.

Code availability

The custom code and analyses are available at https://github.com/umarmohan/freerecall_travelingwaves.

References

1. Ermentrout, G. B. & Kleinfeld, D. Traveling electrical waves in cortex: insights from phase dynamics and speculation on a computational role. *Neuron* **29**, 33–44 (2001).
2. Muller, L., Chavane, Frédéric, Reynolds, J. & Sejnowski, T. J. Cortical travelling waves: mechanisms and computational principles. *Nat. Rev. Neurosci.* **19**, 255–268 (2018).
3. Lubenov, E. V. & Siapas, A. G. Hippocampal theta oscillations are travelling waves. *Nature* **459**, 534–539 (2009).
4. Davis, Z. W., Muller, L., Martinez-Trujillo, J., Sejnowski, T. & Reynolds, J. H. Spontaneous travelling cortical waves gate perception in behaving primates. *Nature* **587**, 432–436 (2020).
5. Benucci, A., Frazor, R. A. & Carandini, M. Standing waves and traveling waves distinguish two circuits in visual cortex. *Neuron* **55**, 103–117 (2007).
6. Hamid, A. A., Frank, M. J. & Moore, C. I. Wave-like dopamine dynamics as a mechanism for spatiotemporal credit assignment. *Cell* **184**, 2733–2749 (2021).
7. Hernández-Pérez, J. Jesús, Cooper, K. W. & Newman, E. L. Medial entorhinal cortex activates in a traveling wave in the rat. *eLife* **9**, e52289 (2020).
8. Bahramisharif, A. et al. Propagating neocortical gamma bursts are coordinated by traveling alpha waves. *J. Neurosci.* **33**, 18849–18854 (2013).
9. Zhang, H., Watrous, A. J., Patel, A. & Jacobs, J. Theta and alpha oscillations are traveling waves in the human neocortex. *Neuron* **98**, 1269–1281.e4 (2018).
10. Alexander, D. M. et al. Traveling waves and trial averaging: the nature of single-trial and averaged brain responses in large-scale cortical signals. *NeuroImage* **73**, 95–112 (2013).
11. Sato, T. K., Nauhaus, I. & Carandini, M. Traveling waves in visual cortex. *Neuron* **75**, 218–229 (2012).
12. Adrian, E. D. & Matthews, B. H. C. The Berger rhythm: potential changes from the occipital lobes in man. *Brain* **57**, 355–385 (1934).
13. Nauhaus, I., Busse, L., Carandini, M. & Ringach, D. L. Stimulus contrast modulates functional connectivity in visual cortex. *Nat. Neurosci.* **12**, 70–76 (2009).
14. Muller, L., Reynaud, A., Chavane, F. & Destexhe, A. The stimulus-evoked population response in visual cortex of awake monkey is a propagating wave. *Nat. Commun.* **5**, 3675 (2014).
15. Muller, L. et al. Rotating waves during human sleep spindles organize global patterns of activity that repeat precisely through the night. *eLife* **5**, e17267 (2016).
16. Massimini, M., Huber, R., Ferrarelli, F., Hill, S. & Tononi, G. The sleep slow oscillation as a traveling wave. *J. Neurosci.* **24**, 6862–6870 (2004).
17. Takahashi, K. et al. Large-scale spatiotemporal spike patterning consistent with wave propagation in motor cortex. *Nat. Commun.* **6**, 7169 (2015).
18. Roberts, J. A. et al. Metastable brain waves. *Nat. Commun.* **10**, 1056 (2019).
19. Bhattacharya, S., Cauchois, M. B. L., Iglesias, P. A. & Chen, Z. S. The impact of a closed-loop thalamocortical model on the spatiotemporal dynamics of cortical and thalamic traveling waves. *Sci. Rep.* **11**, 14359 (2021).
20. Kopell, N. J., Gritton, H. J., Whittington, M. A. & Kramer, M. A. Beyond the connectome: the dynome. *Neuron* **83**, 1319–1328 (2014).
21. Breakspear, M. Dynamic models of large-scale brain activity. *Nat. Neurosci.* **20**, 340–352 (2017).
22. Salinas, E. & Sejnowski, T. J. Correlated neuronal activity and the flow of neural information. *Nat. Rev. Neurosci.* **2**, 539–550 (2001).
23. Alamia, A. & VanRullen, R. Alpha oscillations and traveling waves: signatures of predictive coding? *PLoS Biol.* **17**, e3000487 (2019).
24. Pang, Z., Alamia, A. & VanRullen, R. Turning the stimulus on and off changes the direction of α traveling waves. *eNeuro* **7**, ENEURO.0218-20.2020 (2020).
25. Alamia, A., Terral, L., d'Ambra, M. R. & Van Rullen, R. Distinct roles of forward and backward alpha-band waves in spatial visual attention. *eLife* **12**, e85035 (2023).
26. Engel, A., Fries, P. & Singer, W. Dynamic predictions: oscillations and synchrony in top-down processing. *Nat. Rev. Neurosci.* **2**, 704–716 (2001).
27. Linde-Domingo, J., Treder, M. S., Kerrén, C. & Wimber, M. Evidence that neural information flow is reversed between object perception and object reconstruction from memory. *Nat. Commun.* **10**, 179 (2019).

28. Sederberg, P. B., Kahana, M. J., Howard, M. W., Donner, E. J. & Madsen, J. R. Theta and gamma oscillations during encoding predict subsequent recall. *J. Neurosci.* **23**, 10809–10814 (2003).
29. Burke, J. F. et al. Synchronous and asynchronous theta and gamma activity during episodic memory formation. *J. Neurosci.* **33**, 292–304 (2013).
30. Fisher, N. I. *Statistical Analysis of Circular Data* (Cambridge Univ. Press, 1993).
31. Zhang, H. & Jacobs, J. Traveling theta waves in the human hippocampus. *J. Neurosci.* **35**, 12477–12487 (2015).
32. Polyn, S. M., Norman, K. A. & Kahana, M. J. A context maintenance and retrieval model of organizational processes in free recall. *Psychol. Rev.* **116**, 129–156 (2009).
33. Burke, J. F. et al. Human intracranial high-frequency activity maps episodic memory formation in space and time. *NeuroImage* **85**, 834–843 (2014).
34. Canolty, R. T. et al. High gamma power is phase-locked to theta oscillations in human neocortex. *Science* **313**, 1626–1628 (2006).
35. Jacobs, J., Kahana, M. J., Ekstrom, A. D. & Fried, I. Brain oscillations control timing of single-neuron activity in humans. *J. Neurosci.* **27**, 3839–3844 (2007).
36. Luczak, A., McNaughton, B. L. & Harris, K. D. Packet-based communication in the cortex. *Nat. Rev. Neurosci.* **16**, 745–755 (2015).
37. Hahn, G., Ponce-Alvarez, A., Deco, G., Aertsen, A. & Kumar, A. Portraits of communication in neuronal networks. *Nat. Rev. Neurosci.* **20**, 117–127 (2019).
38. Heitmann, S., Boonstra, T. & Breakspear, M. A dendritic mechanism for decoding traveling waves: principles and applications to motor cortex. *PLoS Comput. Biol.* **9**, e1003260 (2013).
39. Sato, N. Cortical traveling waves reflect state-dependent hierarchical sequencing of local regions in the human connectome network. *Sci. Rep.* **12**, 334 (2022).
40. Sherfey, J., Ardid, S., Miller, E. K., Hasselmo, M. E. & Kopell, N. J. Prefrontal oscillations modulate the propagation of neuronal activity required for working memory. *Neurobiol. Learn. Mem.* **173**, 107228 (2020).
41. Girard, P., Hupé, J. M. & Bullier, J. Feedforward and feedback connections between areas v1 and v2 of the monkey have similar rapid conduction velocities. *J. Neurophysiol.* **85**, 1328–1331 (2001).
42. González-Burgos, G., Barrionuevo, G. & Lewis, D. A. Horizontal synaptic connections in monkey prefrontal cortex: an in vitro electrophysiological study. *Cereb. Cortex* **10**, 82–92 (2000).
43. Chiang, Chia-Chu, Shivacharan, R. S., Wei, X., Gonzalez-Reyes, L. E. & Durand, D. M. Slow periodic activity in the longitudinal hippocampal slice can self-propagate non-synaptically by a mechanism consistent with ephaptic coupling. *J. Physiol.* **597**, 249–269 (2019).
44. Kleen, J. K. et al. Bidirectional propagation of low frequency oscillations over the human hippocampal surface. *Nat. Commun.* **12**, 2764 (2021).
45. Heitmann, S., Gong, P. & Breakspear, M. A computational role for bistability and traveling waves in motor cortex. *Front. Comput. Neurosci.* **6**, 67 (2012).
46. Zabeh, E., Foley, N. C., Jacobs, J. & Gottlieb, J. P. Beta traveling waves in monkey frontal and parietal areas encode recent reward history. *Nat. Commun.* **14**, 5428 (2023).
47. Place, R., Farovik, A., Brockmann, M. & Eichenbaum, H. Bidirectional prefrontal–hippocampal interactions support context-guided memory. *Nat. Neurosci.* **19**, 992–994 (2016).
48. Tomita, H., Ohbayashi, M., Nakahara, K., Hasegawa, I. & Miyashita, Y. Top-down signal from prefrontal cortex in executive control of memory retrieval. *Nature* **401**, 699–703 (1999).
49. Rajasethupathy, P. et al. Projections from neocortex mediate top-down control of memory retrieval. *Nature* **526**, 653–659 (2015).
50. Felleman, D. J. & Van Essen, D. C. Distributed hierarchical processing in the primate cerebral cortex. *Cereb. Cortex* **1**, 1–47 (1991).
51. Markov, N. T. et al. Anatomy of hierarchy: feedforward and feedback pathways in macaque visual cortex. *J. Comp. Neurol.* **522**, 225–259 (2014).
52. Bastos, A. M. et al. Visual areas exert feedforward and feedback influences through distinct frequency channels. *Neuron* **85**, 390–401 (2015).
53. Fries, P. Rhythms for cognition: communication through coherence. *Neuron* **88**, 220–235 (2015).
54. Buffalo, E. A., Fries, P., Landman, R., Liang, H. & Desimone, R. A backward progression of attentional effects in the ventral stream. *Proc. Natl Acad. Sci. USA* **107**, 361–365 (2010).
55. Friston, K. Hierarchical models in the brain. *PLoS Comput. Biol.* **4**, e1000211 (2008).
56. Rubino, D., Robbins, K. A. & Hatsopoulos, N. G. Propagating waves mediate information transfer in the motor cortex. *Nat. Neurosci.* **9**, 1549–1557 (2006).
57. Balasubramanian, K. et al. Propagating motor cortical dynamics facilitate movement initiation. *Neuron* **106**, 526–536 (2020).
58. Bhattacharya, S., Brincat, S. L., Lundqvist, M. & Miller, E. K. Traveling waves in the prefrontal cortex during working memory. *PLoS Comput. Biol.* **18**, e1009827 (2022).
59. Li, J. et al. Anterior–posterior hippocampal dynamics support working memory processing. *J. Neurosci.* **42**, 443–453 (2021).
60. Michalareas, G. et al. Alpha-beta and gamma rhythms subserve feedback and feedforward influences among human visual cortical areas. *Neuron* **89**, 384–397 (2016).
61. Contreras, D., Destexhe, A., Sejnowski, T. J. & Steriade, M. Spatiotemporal patterns of spindle oscillations in cortex and thalamus. *J. Neurosci.* **17**, 1179–1196 (1997).
62. Muller, L. & Destexhe, A. Propagating waves in thalamus, cortex and the thalamocortical system: experiments and models. *J. Physiol. Paris* **106**, 222–238 (2012).
63. Halgren, M. et al. The generation and propagation of the human alpha rhythm. *Proc. Natl Acad. Sci. USA* **116**, 23772–23782 (2019).
64. Breakspear, M., Heitmann, S. & Daffertshofer, A. Generative models of cortical oscillations: neurobiological implications of the Kuramoto model. *Front. Hum. Neurosci.* **4**, 190 (2010).
65. Fries, P., Reynolds, J. H., Rorie, A. E. & Desimone, R. Modulation of oscillatory neuronal synchronization by selective visual attention. *Science* **291**, 1560–1563 (2001).
66. Barzegaran, E. & Plomp, G. Four concurrent feedforward and feedback networks with different roles in the visual cortical hierarchy. *PLoS Biol.* **20**, e3001534 (2022).
67. King, J.-R. & Wyart, V. The human brain encodes a chronicle of visual events at each instant of time through the multiplexing of traveling waves. *J. Neurosci.* **41**, 7224–7233 (2021).
68. Hanslmayr, S., Volberg, G., Wimber, M., Dalal, S. S. & Greenlee, M. W. Prestimulus oscillatory phase at 7 Hz gates cortical information flow and visual perception. *Curr. Biol.* **23**, 2273–2278 (2013).
69. Sauseng, P. et al. EEG alpha synchronization and functional coupling during top-down processing in a working memory task. *Hum. Brain Mapp.* **26**, 148–155 (2005).
70. Hanslmayr, S. et al. The relationship between brain oscillations and BOLD signal during memory formation: a combined EEG–fMRI study. *J. Neurosci.* **31**, 15674–15680 (2011).
71. Busch, N. A., Dubois, J. & Van Rullen, R. The phase of ongoing EEG oscillations predicts visual perception. *J. Neurosci.* **29**, 7869–7876 (2009).
72. Mathewson, K. E., Gratton, G., Fabiani, M., Beck, D. M. & Ro, T. To see or not to see: prestimulus α phase predicts visual awareness. *J. Neurosci.* **29**, 2725–2732 (2009).
73. Dugué, L., Marque, P. & Van Rullen, R. The phase of ongoing oscillations mediates the causal relation between brain excitation and visual perception. *J. Neurosci.* **31**, 11889–11893 (2011).

74. Patten, T. M., Rennie, C. J., Robinson, P. A. & Gong, P. Human cortical traveling waves: dynamical properties and correlations with responses. *PLoS ONE* **7**, e38392 (2012).
75. Lozano-Soldevilla, D. & Van Rullen, R. The hidden spatial dimension of alpha: 10-Hz perceptual echoes propagate as periodic traveling waves in the human brain. *Cell Rep.* **26**, 374–380 (2019).
76. Stolk, A. et al. Electrocorticographic dissociation of alpha and beta rhythmic activity in the human sensorimotor system. *eLife* **8**, e48065 (2019).
77. Kastner, S., Pinsk, M. A., De Weerd, P., Desimone, R. & Ungerleider, L. G. Increased activity in human visual cortex during directed attention in the absence of visual stimulation. *Neuron* **22**, 751–761 (1999).
78. Buschman, T. J. & Miller, E. K. Top-down versus bottom-up control of attention in the prefrontal and posterior parietal cortices. *Science* **315**, 1860–1862 (2007).
79. Gazzaley, A. & Nobre, A. C. Top-down modulation: bridging selective attention and working memory. *Trends Cogn. Sci.* **16**, 129–135 (2012).
80. Haegens, S., Cousijn, H., Wallis, G., Harrison, P. J. & Nobre, A. C. Inter- and intra-individual variability in alpha peak frequency. *NeuroImage* **92**, 46–55 (2014).
81. Mahjoory, K., Schoffelen, J.-M., Keitel, A. & Gross, J. The frequency gradient of human resting-state brain oscillations follows cortical hierarchies. *eLife* **9**, e53715 (2020).
82. Mueller, S. et al. Individual variability in functional connectivity architecture of the human brain. *Neuron* **77**, 586–595 (2013).
83. Pang, J. C. et al. Geometric constraints on human brain function. *Nature* **618**, 566–574 (2023).
84. Fischl, B. R., Sereno, M. I., Tootell, R. B. H. & Dale, A. M. High-resolution inter-subject averaging and a coordinate system for the cortical surface. *Hum. Brain Mapp.* **8**, 272–284 (1999).
85. Steinmetz, N. A., Koch, C., Harris, K. D. & Carandini, M. Challenges and opportunities for large-scale electrophysiology with neuropixels probes. *Curr. Opin. Neurobiol.* **50**, 92–100 (2018).
86. Khodagholy, D. et al. Neurogrid: recording action potentials from the surface of the brain. *Nat. Neurosci.* **18**, 310–315 (2015).
87. Ribary, U. et al. Magnetic field tomography of coherent thalamocortical 40-Hz oscillations in humans. *Proc. Natl Acad. Sci. USA* **88**, 11037–11041 (1991).
88. Boto, E. et al. A new generation of magnetoencephalography: room temperature measurements using optically-pumped magnetometers. *NeuroImage* **149**, 404–414 (2017).
89. Said, C. P., Egan, R. D., Minshew, N. J., Behrmann, M. & Heeger, D. J. Normal binocular rivalry in autism: implications for the excitation/inhibition imbalance hypothesis. *Vis. Res.* **77**, 59–66 (2013).
90. Smith, E. H. et al. Human interictal epileptiform discharges are bidirectional traveling waves echoing ictal discharges. *eLife* **11**, e73541 (2022).
91. Talairach, J. & Tournoux, P. *Co-planar Stereotaxic Atlas of the Human Brain* (G. Thieme, 1988).
92. Das, A. et al. Spontaneous neuronal oscillations in the human insula are hierarchically organized traveling waves. *eLife* **11**, e76702 (2022).
93. Berens, P. Circstat: a MATLAB toolbox for circular statistics. *J. Stat. Softw.* **31**, 1–21 (2009).
94. Kempter, R., Leibold, C., Buzsáki, G., Diba, K. & Schmidt, R. Quantifying circular–linear associations: hippocampal phase precession. *J. Neurosci. Methods* **207**, 113–124 (2012).
95. Masseran, N., Razali, A. M., Ibrahim, K. & Latif, M. T. Fitting a mixture of von Mises distributions in order to model data on wind direction in peninsular Malaysia. *Energy Convers. Manage.* **72**, 94–102 (2013).
96. Oostenveld, R., Fries, P., Maris, E. & Schoffelen, J.-M. Fieldtrip: open source software for advanced analysis of MEG, EEG, and invasive electrophysiological data. *Comput. Intell. Neurosci.* **2011**, 156869 (2011).
97. Maris, E. & Oostenveld, R. Nonparametric statistical testing of EEG- and MEG-data. *J. Neurosci. Methods* **164**, 177–190 (2007).
98. Benjamini, Y. & Hochberg, Y. Controlling the false discovery rate: a practical and powerful approach to multiple testing. *J. R. Stat. Soc. B* **57**, 289–300 (1995).
99. Nilearn contributors. nilearn. *GitHub* https://github.com/nilearn/nilearn (2007–2023).
100. Abraham, A. et al. Machine learning for neuroimaging with scikit-learn. *Front. Neuroinform.* **8**, 14 (2014).

Acknowledgements

We thank the patients for participating in our study. This work was supported by the DARPA Restoring Active Memory programme (Cooperative Agreement No. N66001-14-2-4032); National Institutes of Health Grant Nos R01-MH104606, U01-NS113198 and RF1-MH114276; and the National Science Foundation (to J.J.). The views, opinions and/or findings expressed are those of the authors and should not be interpreted as representing the official views or policies of the Department of Defense or the US government. The funders had no role in study design, data collection and analysis, decision to publish or preparation of the manuscript. We thank J. Chapeton, A. Das, T. Donoghue, M. Hermiller, L. Kunz, S. Favila, J. Gottlieb, B. Lega, S. Qasim and E. Zabeh for providing helpful critical feedback on the manuscript. We thank M. Kahana, P. Wanda and J. Rudoler for providing data and technical support.

Author contributions

U.R.M., H.Z., B.E. and J.J. designed and implemented the data analyses. U.R.M., B.E. and J.J. wrote the manuscript.

Competing interests

The authors declare no competing interests.

Additional information

Extended data is available for this paper at https://doi.org/10.1038/s41562-024-01838-3.

Supplementary information The online version contains supplementary material available at https://doi.org/10.1038/s41562-024-01838-3.

Correspondence and requests for materials should be addressed to Joshua Jacobs.

Peer review information *Nature Human Behaviour* thanks Ziv Williams and the other, anonymous, reviewer(s) for their contribution to the peer review of this work. Peer reviewer reports are available.

https://doi.org/10.1038/s41562-024-01838-3

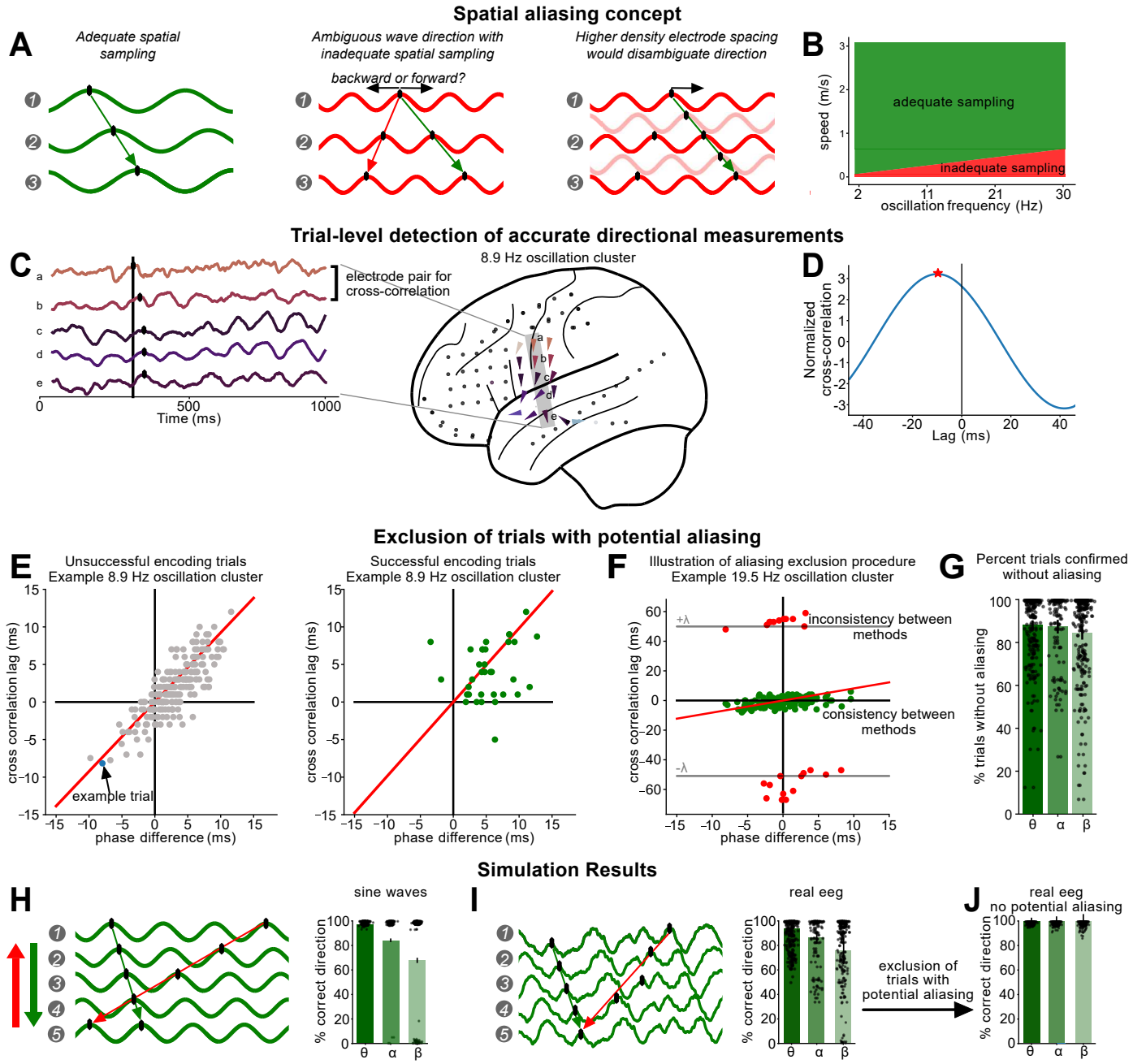

Extended Data Fig. 1 | Exclusion of trials with potential inaccurate measurement of propagation direction due to spatial aliasing. (A) Adequate spatial sampling when low-frequency oscillations propagate propagate across 3 widely spaced electrodes(left). Inadequate spatial sampling for higher-frequency oscillations propagating across 3 electrodes with the same spacing (middle). Arrows indicate two possible propagation direction measurements. Higher density electrode spacing would disambiguate the true propagation direction (right). (B) Combinations of oscillation frequencies and phase velocities where there is adequate and inadequate spatial sampling with 1 cm electrode spacing, determined by whether half the spatial wavelength of a propagating oscillation is less than 1 cm, shown in green and red, respectively. (C) Example 1 s of a trial with a traveling wave propagating in space across five adjacent electrodes of an alpha oscillation cluster in patient 34. (D) Time-lagged cross correlation for entire trial measured between adjacent electrodes (a) and (b) in oscillation cluster. Time of maximum coupling measured at -11 ms indicated by red star showing signal on electrode (b) leads electrode (a). (E) Correlation between time differences between electrodes (a) and (b) measured via phase differences with the time-lag measured from cross-correlation for unsuccessful encoding trial son the left and successful encoding trials on the right. Strong correlation along unity lines indicates alignment between the two measurements such that no trials were susceptible to spatial aliasing. (F) Correlation between phase-based time differences and correlation-based time differences for a beta oscillation cluster with 18% of trials showing an inconsistency between the two methods. Red time lags measured via cross-correlation indicate that the true lag between the signals on those trials was approximately a cycle forward or backwards indicating the potential for spatial aliasing when measuring only using phase. (G) When excluding trials with these inconsistencies across all clusters in the dataset, approximately 83% of trials were not susceptible to spatial aliasing (right) across all oscillation clusters (n=421). Error bars denote ± 1 SEM. (H) Percent of trials in which the correct direction could be measured using phase differences when perfect sinusoidal signals were shifted across five simulated electrodes (n=421). (I) Percent of trials in which the correct direction could be measured using phase differences when imperfect eeg signals were shifted across five simulated electrodes (n=421). (J) Percent of trials in which the correct direction could be measured using phase differences when real eeg signals were shifted across five simulated electrodes after excluding trials that were susceptible to spatial aliasing (n=421).

https://doi.org/10.1038/s41562-024-01838-3

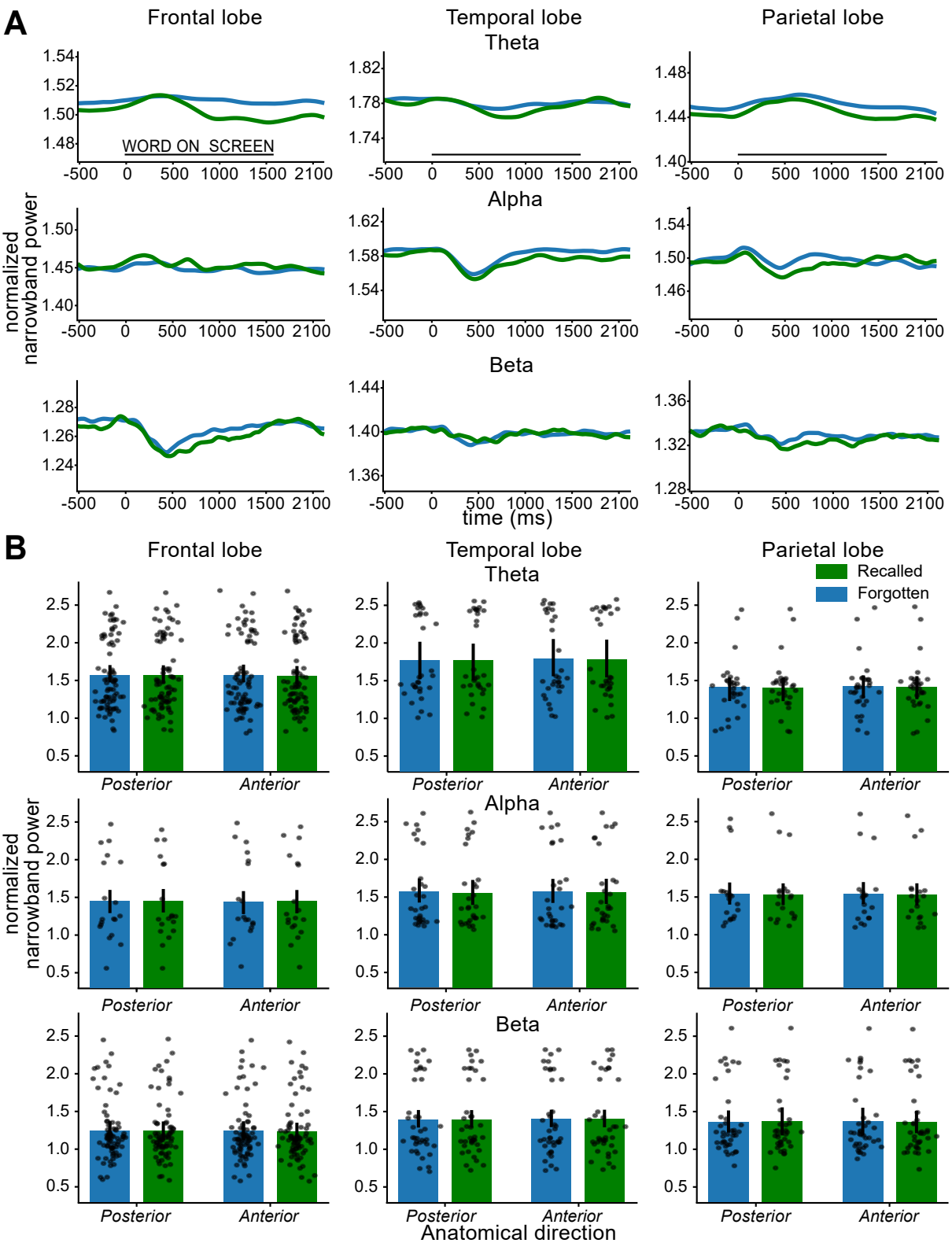

Extended Data Fig. 2 | Narrowband power at oscillation clusters that showed traveling waves in the episodic memory task. (A) Mean normalized narrowband power centered around each oscillation cluster's peak frequency across all 93 participants, calculated with the log-transformed amplitude of the Hilbert transform prior to selecting trials with sufficient oscillatory power, wave strength, and no potential for spatial aliasing. (B) Mean normalized narrowband power for oscillation clusters that showed traveling waves averaged over time in all 93 participants, separately calculated during time periods when TWs moved posteriorly and anteriorly, during successful and unsuccessful encoding trials. There were no significant differences in mean power across the clusters that showed posterior and anterior propagation (all p's > 0.05, two-sided *t*-test). Error bars denote ± 1 SEM.

https://doi.org/10.1038/s41562-024-01838-3

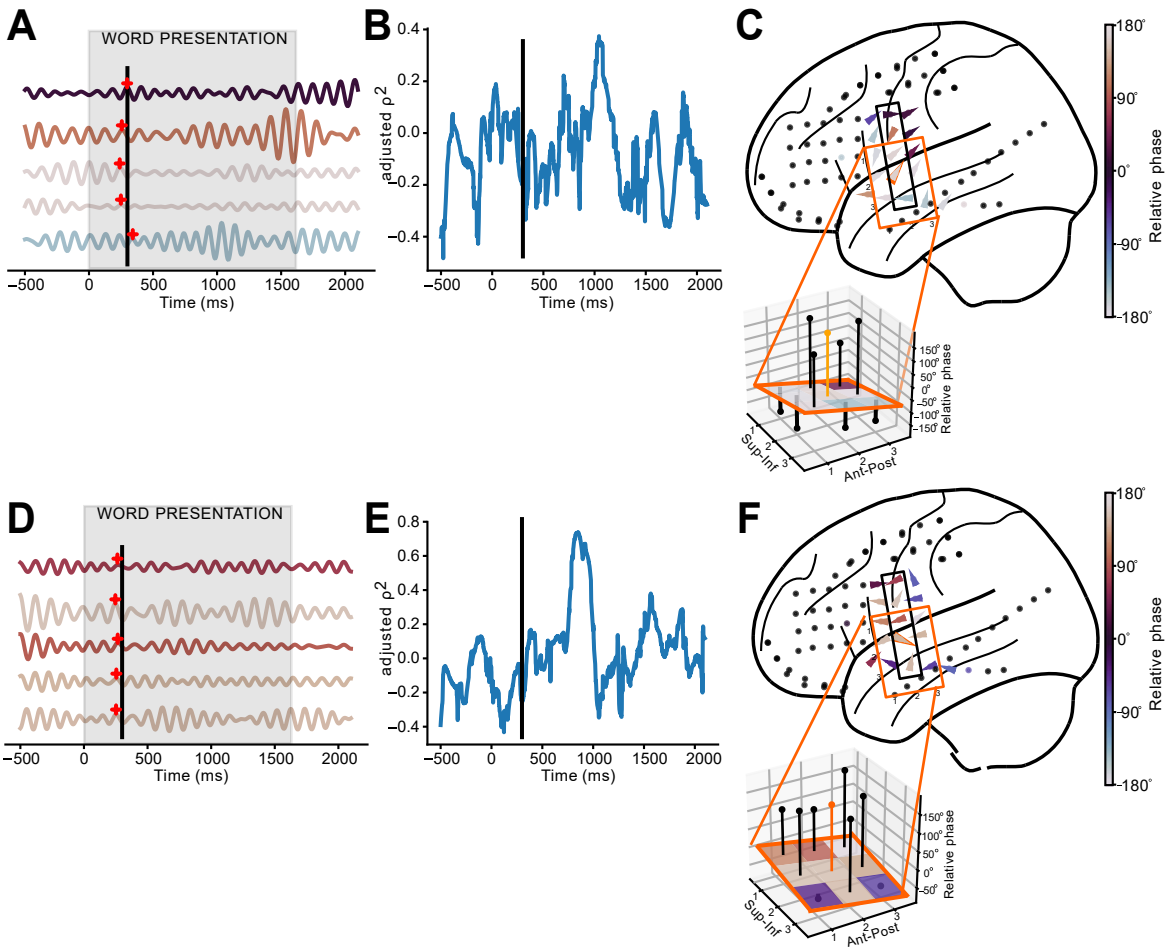

Extended Data Fig. 3 | Example data showing the absence of traveling waves. (A) Example trial where a traveling wave was not present on a cluster that often showed 8.9-Hz oscillations that propagated as TWs on other trials. Filtered signals from five channels during one trial of memory task from participant 34. (B) Timecourse of adjusted r^2 across the cluster used to measure statistical reliability of circular-linear models fit to the phase gradients. (C) Brain map with arrows indicating, for each electrode, the calculated local propagation direction. Arrow color indicates relative phase at time indicated by black line in A. (D-F) Same as (A-C) for additional example trial.

https://doi.org/10.1038/s41562-024-01838-3

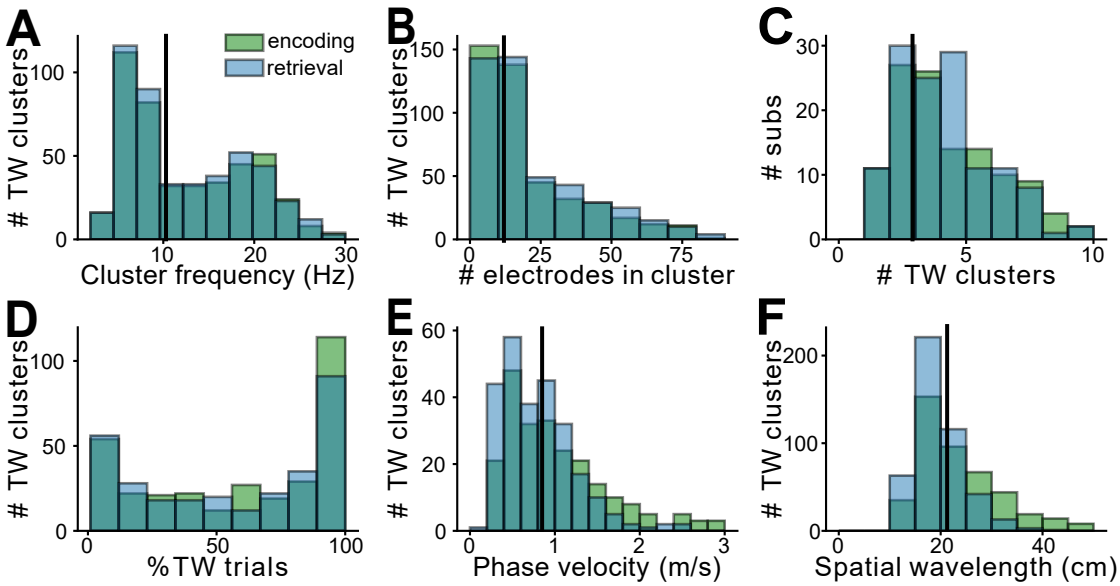

Extended Data Fig. 4 | Characteristics of cortical traveling waves during encoding and recall of episodic memory task. (A) Histogram of the peak oscillation frequencies for clusters with TWs. All green histograms are properties measured during encoding and blue during recall. (B) Histogram of the number of electrodes in each cluster. (C) Histogram of the counts of clusters per patient that showed TWs. Most participants had 2 to 4 clusters across different sets of grid and strip electrodes or groups of electrodes with oscillations at different peak frequencies. A few patients had 5 or more. Patients with many clusters often had multiple smaller clusters of 5-6 electrodes in different regions and hemispheres. (D) Distribution of the percentage of single trials that show reliable TWs for individual clusters. (E) Histogram of TW propagation phase velocities across clusters. Black line indicates median. (F) Histogram of TW spatial wavelength.

https://doi.org/10.1038/s41562-024-01838-3

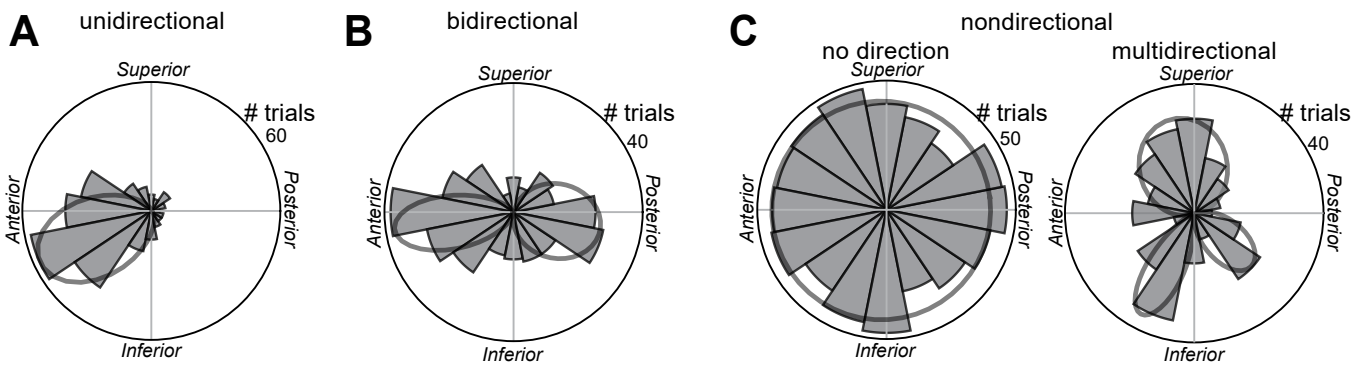

Extended Data Fig. 5 | Examples of clusters that showed traveling waves with different types of directional propagation patterns. Plots show example direction distribution for TWs we labeled as propagating in (A) unidirectional, (B) bidirectional, and (C) nondirectional fashions.

https://doi.org/10.1038/s41562-024-01838-3

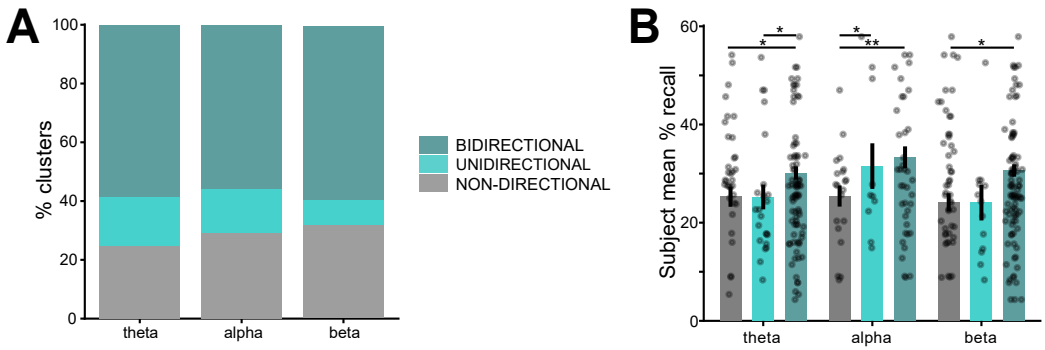

Extended Data Fig. 6 | Population categorization of cluster direction patterns in episodic memory task. (A) Percent of TW clusters in each oscillatory range identified as bidirectional, unidirectional, and nondirectional across all 93 participants. (B) Mean percent recall rates across 93 participants that showed a TW cluster with unidirectional, bidirectional, and nondirectional TW propagation, by oscillatory frequency band (linear mixed effects model, bidirectional vs. unidirectional clusters: p=0.062; bidirectional vs. nondirectional TW clusters:, p=0.002, Tukey contrast multiple comparisons test). Error bars denote ± 1 SEM. (*p < 0.05, ** p < 0.01, two-sided *t*-test). Overall, participants who showed bidirectional TW propagation showed a 5.8% higher rate of successful memory encoding compared to participants with unidirectional and multidirectional patterns, indicating that bidirectional TW propagation may be a feature of normal cognition.

https://doi.org/10.1038/s41562-024-01838-3

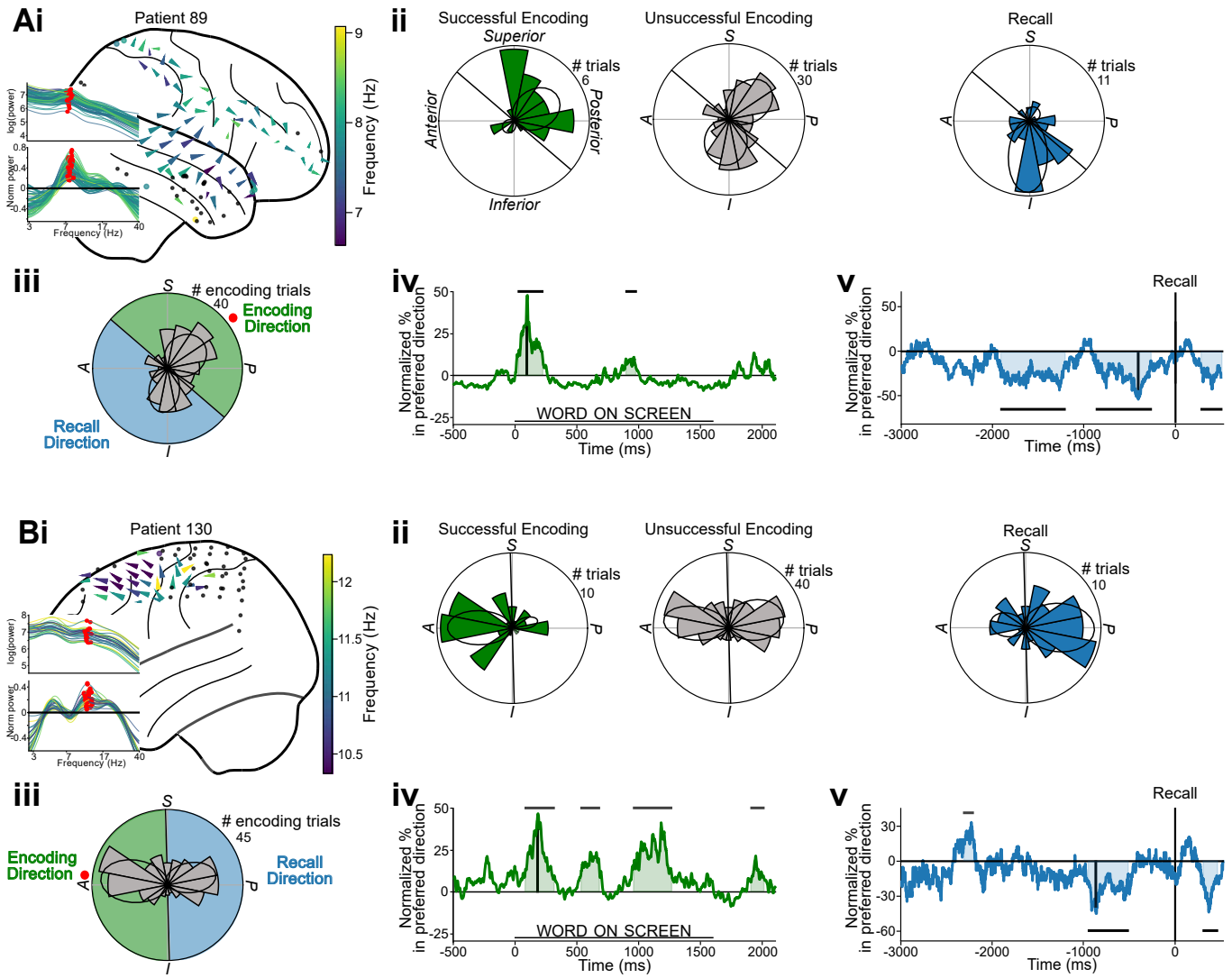

Extended Data Fig. 7 | Traveling waves in example participants who showed a link between TW direction and memory. (A) Example traveling wave in patient 89 at 7.8 Hz; format of individual plots follows Fig. 3. (B) Example traveling wave frontal cortex of patient 130 at 10.8 Hz.

https://doi.org/10.1038/s41562-024-01838-3

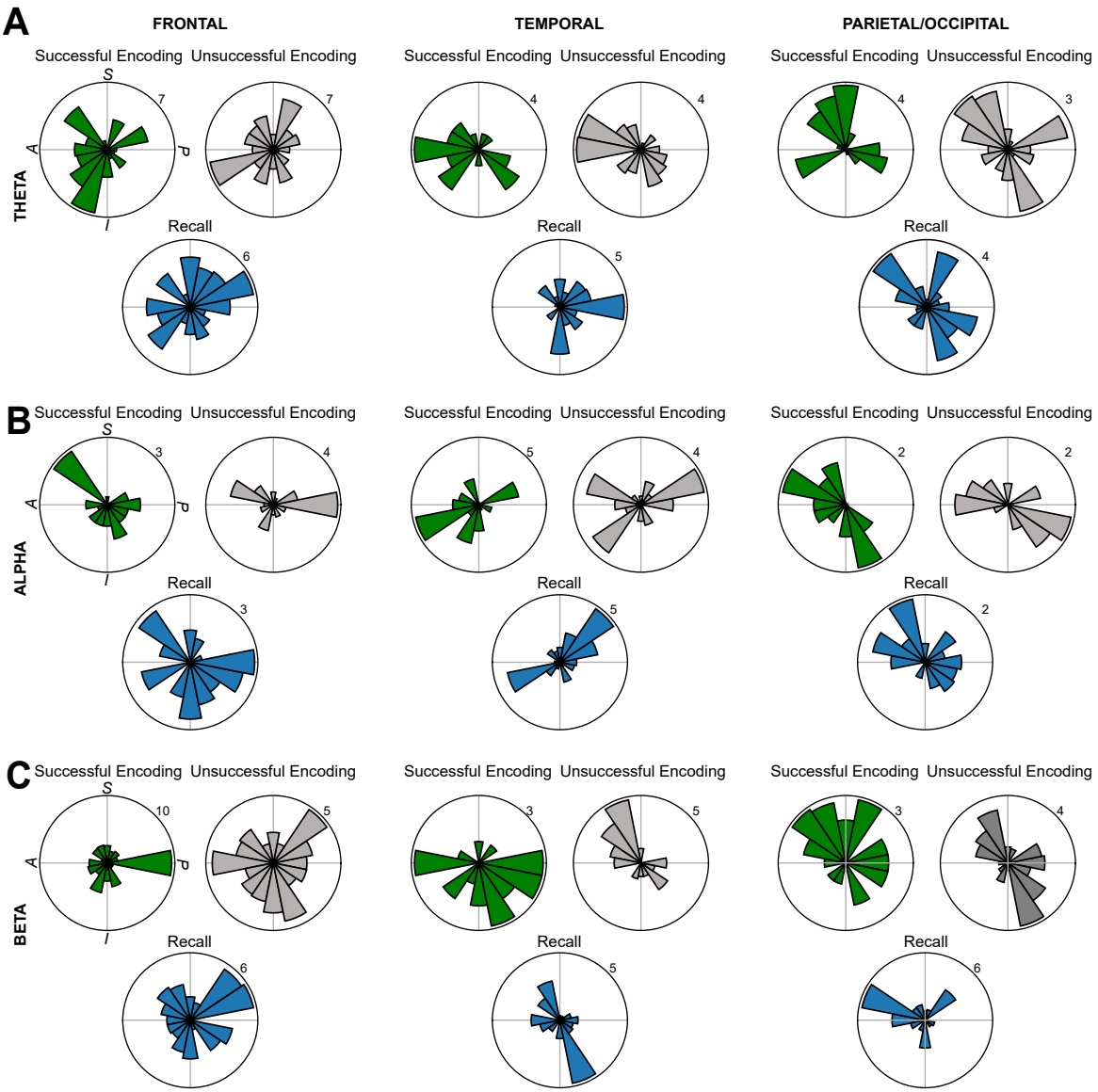

Extended Data Fig. 8 | Direction distributions during memory encoding and recall. (A) Distribution of clusters' pre-dominant propagation directions for all theta TWs measured on oscillation clusters in the Frontal, Temporal, and Parietal/Occipital regions during memory encoding and recall at the timepoint of maximal memory-related effects. TW propagation directions were weighted by the proportion of trials with TWs propagating in each directions captured (see Methods). (B) Same as (A) for alpha-band TWs (C) Same as (A) for beta-band TWs.

https://doi.org/10.1038/s41562-024-01838-3

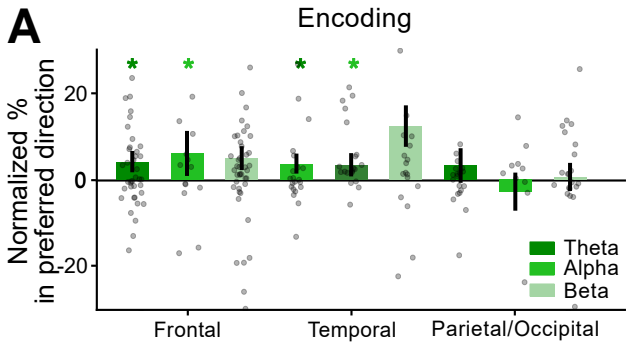

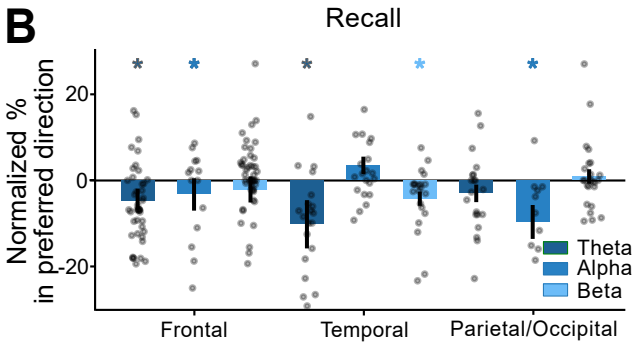

Extended Data Fig. 9 | Relation between TW directional shifts and memory processing. (A) Normalized difference in the prevalence of TWs propagating in the preferred encoding direction versus the opposite direction for successful encoding relative to the cluster's natural bidirecitonal split (averaged across word presentation intervals). Asterisks indicate specific regions and oscillatory bands where the normalized percent of TWs traveling in preferred encoding directions across clusters is significantly above a distribution of shuffled TW directions (p's < 0.05, one-sided binomial tests against 0, Cluster counts in Suplementary Table 1). Error bars denote ± 1 SEM. (B) Normalized difference of TWs propagating in preferred encoding versus preferred recall direction averaged during 2 seconds prior to verbal recall. Asterisks indicate specific regions and oscillatory bands where the normalized percent of TWs traveling in preferred encoding directions across clusters is significantly below a distribution of shuffled TW directions (p's < 0.05, one-sided binomial tests).

https://doi.org/10.1038/s41562-024-01838-3

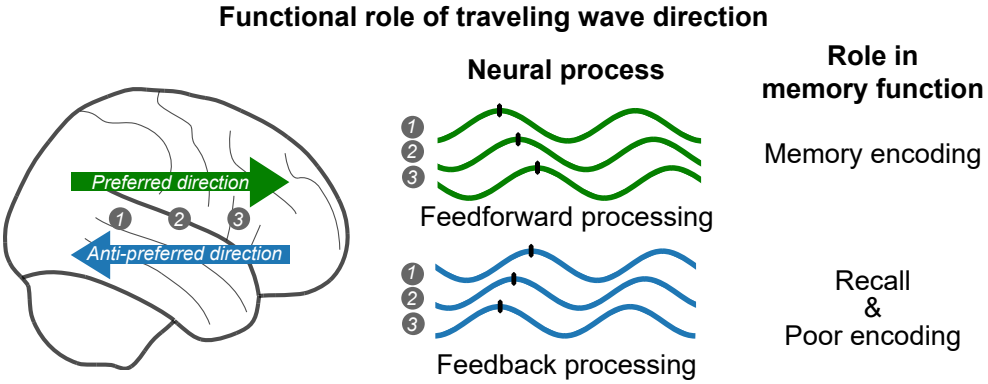

Extended Data Fig. 10 | Hypothesized relations between traveling wave (TW) direction and memory processes. When presented with a list of words during an episodic memory task, successful memory encoding more likely when waves propagated in the preferred encoding direction, as opposed to the opposite direction, characterized as the preferred recall direction. We hypothesize that preferred encoding and preferred recall TW propagation may reflect more general neural processes including feedforward and feedbackward cortical processing, respectively.

nature portfolio

Corresponding author(s): Joshua Jacobs, PhD
Uma Mohan, PhD

Last updated by author(s): Jan 10, 2024

Reporting Summary

Nature Portfolio wishes to improve the reproducibility of the work that we publish. This form provides structure for consistency and transparency in reporting. For further information on Nature Portfolio policies, see our Editorial Policies and the Editorial Policy Checklist.

Statistics

For all statistical analyses, confirm that the following items are present in the figure legend, table legend, main text, or Methods section.

n/a	Confirmed
☐	☒ The exact sample size (*n*) for each experimental group/condition, given as a discrete number and unit of measurement
☐	☒ A statement on whether measurements were taken from distinct samples or whether the same sample was measured repeatedly
☐	☒ The statistical test(s) used AND whether they are one- or two-sided *Only common tests should be described solely by name; describe more complex techniques in the Methods section.*
☐	☒ A description of all covariates tested
☐	☒ A description of any assumptions or corrections, such as tests of normality and adjustment for multiple comparisons
☐	☒ A full description of the statistical parameters including central tendency (e.g. means) or other basic estimates (e.g. regression coefficient) AND variation (e.g. standard deviation) or associated estimates of uncertainty (e.g. confidence intervals)
☐	☒ For null hypothesis testing, the test statistic (e.g. *F*, *t*, *r*) with confidence intervals, effect sizes, degrees of freedom and *P* value noted *Give P values as exact values whenever suitable.*
☒	☐ For Bayesian analysis, information on the choice of priors and Markov chain Monte Carlo settings
☒	☐ For hierarchical and complex designs, identification of the appropriate level for tests and full reporting of outcomes
☐	☒ Estimates of effect sizes (e.g. Cohen's *d*, Pearson's *r*), indicating how they were calculated

Our web collection on statistics for biologists contains articles on many of the points above.

Software and code

Policy information about availability of computer code

Data collection	Data recordings were performed using commercial software for clinical intracranial electroencephalographic recording systems at each hospital (Nihon Kohden EEG-1200, Natus XLTek EMU 128, Natus Quantum EEG, or Grass Aura-LTM64 systems).
Data analysis	Data were analyzed with Python 3.6.7 using its built-in functions as well as publicly available libraries Python Time Series Analysis Toolbox (v. 2.0.3, https://github.com/pennmem/ptsa), CMLReaders toolbox (v. 0.9.3, https://github.com/pennmem/cmlreaders), PyCircStat toolbox (v. 0.0.2), mne (v. 0.19.2), nilearn (v. 0.9.2), FOOOF (v. 1.0.0), and FreeSurfer (v. 7.1.1) . All traveling wave analyses were performed using custom code (https://github.com/jacobslab/Traveling-wave-analysis, https://github.com/umarmohan/freerecall_travelingwaves).

For manuscripts utilizing custom algorithms or software that are central to the research but not yet described in published literature, software must be made available to editors and reviewers. We strongly encourage code deposition in a community repository (e.g. GitHub). See the Nature Portfolio guidelines for submitting code & software for further information.

Data

Policy information about availability of data

All manuscripts must include a data availability statement. This statement should provide the following information, where applicable:

- Accession codes, unique identifiers, or web links for publicly available datasets
- A description of any restrictions on data availability
- For clinical datasets or third party data, please ensure that the statement adheres to our policy

The raw electrophysiological data used in this study are available at http://memory.psych.upenn.edu/RAM.

Research involving human participants, their data, or biological material

Policy information about studies with human participants or human data. See also policy information about sex, gender (identity/presentation), and sexual orientation and race, ethnicity and racism.

Reporting on sex and gender	Individual patients' sex is reported in the supplemental subject table.
Reporting on race, ethnicity, or other socially relevant groupings	Additionally, individual patients' age, handedness, clinical electrode coverage of surface grid and depth electrodes, and locations of electrodes included in the analyses are reported in the supplemental subject table. Race and ethnicity of patients were collected
Population characteristics	48 patients were male and 45 patients were female. All patients in this study were adults with their ages ranging from 19 to 57. Additional data on handedness and clinical electrode coverage are reported in the supplemental subject table.
Recruitment	Collaborating clinical teams at the following hospitals (Thomas Jefferson University Hospital (Philadelphia, PA); University of Texas Southwestern Medical Center (Dallas, TX); Emory University Hospital (Atlanta, GA); Dartmouth–Hitchcock Medical Center (Lebanon, NH); Hospital of the University of Pennsylvania (Philadelphia, PA); Mayo Clinic (Rochester, MN); National Institutes of Health (Bethesda, MD); and Columbia University Hospital (New York, NY)) recruited subjects undergoing treatment for pharmacoresistant epilepsy, and performed clinical duties associated with data collection including neurosurgical procedures and patient monitoring. Data was drawn from this publicly available database, and active recruitment was not a apart of this study.
Ethics oversight	Prior to data collection, research protocols were approved by the Institutional Review Board at participating hospitals (Thomas Jefferson University Hospital, University of Texas Southwestern Medical Center, Emory University Hospital, Dartmouth–Hitchcock Medical Center, Hospital of the University of Pennsylvania, Mayo Clinic, National Institutes of Health, Columbia University Hospital), and informed consent was obtained from each participant. Data acquisition and storage was coordinated by the Data Coordinating Center (DCC) at the University of Pennsylvania (IRB protocol 820553).

Note that full information on the approval of the study protocol must also be provided in the manuscript.

Field-specific reporting

Please select the one below that is the best fit for your research. If you are not sure, read the appropriate sections before making your selection.

☒ Life sciences ☐ Behavioural & social sciences ☐ Ecological, evolutionary & environmental sciences

For a reference copy of the document with all sections, see nature.com/documents/nr-reporting-summary-flat.pdf

Life sciences study design

All studies must disclose on these points even when the disclosure is negative.

Sample size	We analyzed data of 160 subjects (93 showing traveling waves) who were pharmacoresistant epilepsy patients surgically implanted with grids and strips of electrodes on the surface of their cortex for the purpose of identifying epileptogenic regions. Patients performed an episodic-memory task. No statistical methods were used to determine sample size in advance. All patients in the database who performed an episodic memory task and had electrodes implanted on the surface of their cortex were studied.
Data exclusions	Data recording segments with epileptiform discharges or electrical artifact were excluded from analyses. A patient's data were excluded from analyses if they did not show any clusters of at least 5 electrodes with oscillations at the same frequency or if the oscillations clusters did not show reliable traveling waves on a sufficient number of trials. For patients with reliable traveling waves, trials were excluded if they did not show oscillations or if the oscillations present were not spatially organized as traveling waves.
Replication	The main findings were replicated by conducting analyses independently on all subjects with and without the addition of exclusion criteria for specific segments of data. Repetition of permutation and subsampling control analyses further confirmed main findings. Our main findings were replicable across multiple subjects as well as multiple sessions within subjects who performed multiple sessions of the task. Data are publicly available enabling independent researchers to replicate these findings.

Randomization	N/A since subjects were not grouped.
Blinding	N/A since subjects were not grouped.

Reporting for specific materials, systems and methods

We require information from authors about some types of materials, experimental systems and methods used in many studies. Here, indicate whether each material, system or method listed is relevant to your study. If you are not sure if a list item applies to your research, read the appropriate section before selecting a response.

Materials & experimental systems

n/a	Involved in the study
☒	☐ Antibodies
☒	☐ Eukaryotic cell lines
☒	☐ Palaeontology and archaeology
☒	☐ Animals and other organisms
☒	☐ Clinical data
☒	☐ Dual use research of concern
☒	☐ Plants

Methods

n/a	Involved in the study
☒	☐ ChIP-seq
☒	☐ Flow cytometry
☐	☒ MRI-based neuroimaging

Magnetic resonance imaging

Experimental design

Design type	T1 and T2 weighted structural MRIs taken prior to patients being implanted with electrodes. MRIs were taken purely for clinical purposes to indicate electrode locations and were not part of these analyses.
Design specifications	N/A. MRIs were taken purely for clinical purposes to indicate electrode locations and were not part of these analyses.
Behavioral performance measures	N/A. MRIs were taken purely for clinical purposes to indicate electrode locations and were not part of these analyses.

Acquisition

Imaging type(s)	Structural MRI and CT
Field strength	3T MRI prior to electrode implantation and 1.5 T MRI following
Sequence & imaging parameters	Sequence & imaging parameters: Imaging parameters varied somewhat among institutions in this multisite study. In general, sequences required for macroelectrode and microwire localization included 3D Tl-weighted with 1 mm or less isotropic resolution, coronal fast spin echo T2-weighted with 0.4 x 0.4 mm in-plane resolution and 2 mm slice thickness, and CT with less than 1 mm slice thickness. Representative examples are as follows: Pre-implant 3D Tl-weighted MPRAGE (TR 1900 ms, TE 2.52 ms, flip angle 9, 1 mm isotropic resolution, 216 x 256 x 174 matrix), pre-implant coronal FSE T2-weighted (TR 7200 ms, 76 ms, ETL 15, flip angle 139, 0.4 x 0.4 x 2 mm, 448 x 448 x 30), post-implant CT (0.5 x 0.5 x 0.625 mm, 512 x 512 x 384)
Area of acquisition	Tl - whole brain, T2 - temporal lobes spanning and oriented in the coronal plane

Diffusion MRI ☐ Used ☒ Not used

Preprocessing

Preprocessing software	Freesurfer's automated cortical parcellation based on the Desikan-Killiany brain atlas
Normalization	We identified the location of each electrode by co-registering a structural magnetic resonance image (MRI) taken prior to surgery with a computed tomography (CT) image after electrodes were surgically implanted in order align the images to each other using rigid registration based on mutual information with Advanced Normalization Tools (ANTS) software to compute electrode locations in standardized Talairach coordinates
Normalization template	Electrode locations normalized in Talairach coordinates.
Noise and artifact removal	N/A. No noise or artifact removal was used.
Volume censoring	N/A. No volume censor was used.

Statistical modeling & inference

Model type and settings	N/A. No statistical modeling was used as MRIs were taken purely for clinical purposes to indicate electrode locations and were not part of these analyses.
Effect(s) tested	N/A. No effects tested as MRIs were taken purely for clinical purposes to indicate electrode locations and were not part of these analyses.

Specify type of analysis: ☒ Whole brain ☐ ROI-based ☐ Both

Statistic type for inference (See Eklund et al. 2016)	N/A. No inference was performed as MRIs were taken purely for clinical purposes to indicate electrode locations and were not part of these analyses.
Correction	N/A. No correction was performed as MRIs were taken purely for clinical purposes to indicate electrode locations and were not part of these analyses.

Models & analysis

n/a	Involved in the study
☒	☐ Functional and/or effective connectivity
☒	☐ Graph analysis
☒	☐ Multivariate modeling or predictive analysis